Vilnius Gediminas Technical University

Kaunas University of Technology

Bialystok Technical University

Lithuanian Society of Biomechanics

IFToMM National Committee of Lithuania

The 10th International Conference

BIOMDLORE 2013

Abstracts

Sponsors:

Edited by Mečislovas Mariūnas and Julius Griškevičius

20–22 September, 2013
Palanga, Lithuania

Vilnius „Technika“ 2013

10th International Conference "BIOMDLORE 2013". Abstracts of Papers for the 10th International Conference: BIOMDLORE 2013. Palanga, Lithuania, 20–22 September, 2013. Edited by Mečislovas Mariūnas and Julius Griškevičius. Vilnius: Technika, 2013. 62 p.

SCOPE OF THE CONFERENCE
Biomechanics
Locomotion
Orthopedics and Traumatology
Compensatory Equipment
Rehabilitation
Medical Diagnostics
Biosignal's Analysis
Mathematical Modeling

Abstracts were qualified on the basis of critical reviews

BIOMDLORE 2013 organized by:

Vilnius Gediminas Technical University
Kaunas University of Technology
Bialystok Technical University
Lithuanian Society of Biomechanics
IFToMM National Committee of Lithuania

This is a science literature book No 2164-M,
issued by VGTU Press TECHNIKA
http://leidykla.vgtu.lt

eISSN 2345-0630
ISBN 978-609-457-548-8
eISBN 978-609-457-550-1
doi: 10.3846/2164-M

12/09/2013. 7,75 printer's sheets.
Print-on-Demand.
Published by Vilnius Gediminas Technical University Press Technika (Saulėtekio al. 11, LT-10223 Vilnius, *Lithuania,*
http://vgtu.leidykla.lt

SCIENTIFIC COMMITTEE

Chairman
Prof. M. MARIŪNAS (Lithuania)

Co-chairmen:
Prof. R.T. TOLOČKA (Lithuania)
Prof. J.R. DĄBROWSKI (Poland)

Secretary:
Assoc. Prof. A. ŠEŠOK (Lithuania)

Members:
Academician A. SVIRIDENOK (Belarus)
Prof. C. FRIGO (Italy)
Prof. S. J. BOLTRUKIEWICZ (Belarus)
Prof. R. BĘDZINSKI (Poland)
Prof. K. KĘDZIOR (Poland)
Prof. Y.M. HADDAD (Canada)
Prof. V. LAURUŠKA (Lithuania)
Prof. K. SIBILSKI (Poland)
Prof. G. ŽILIUKAS (Lithuania)
Prof. P. ŽILIUKAS (Lithuania)
PD Dr. K.-U. SCHMITT (Switzerland)
Assoc. Prof. D. SATKUNSKIENĖ (Lithuania)
Prof. V. TREGUBOV (Russia)
Prof. I. KNETS (Latvia)
MD. Dr. J. CWANEK (Poland)
Prof. A. RUGGIERO (Italy)
MD. Dr. J. BROŽAITIENĖ (Lithuania)
Prof. K.J. VAN ZWIETEN (Belgium)
Dr. P.M. AUBIN (USA)
Assoc. Prof. N. KIZILOVA (Ukraine)
Prof. V. LAURUTIS (Lithuania)

ORGANIZING COMMITTEE

Chairman:
Assoc. Prof. J. GRIŠKEVIČIUS (Lithuania)

Co-Chairman:
Assoc. Prof. V. EIDUKYNAS (Lithuania)

Secretary:
J. ŽIŽIENĖ (Lithuania)
Assoc. Prof. J. PAUK (Poland)

Members:
Assoc. Prof. K. DAUNORAVIČIENĖ (Lithuania)
Assoc. Prof. A. ŠEŠOK (Lithuania)
G. JONAITIS (Lithuania)

Contents

Preface

The main goals of this conference are to create a forum for scientists to present their latest research results in fields of biomechanics and biomedical engineering and to establish new contacts.

„We would like to invite all scientists, engineers, physicians and entrepreneurs who work in broad fields of biomechanics and biomedical engineering to share their knowledge, to gain experience and to build new relationships."

MEČISLOVAS MARIŪNAS
Scientific Chairman of the International Conference
BIOMDLORE 2013

Factors affecting improvement in exercise capacity in patients undergoing cardiac rehabilitation program

J. Brožaitienė[1], I. Duonelienė[2], B. Vaičiūnienė[3], M. Staniūtė[4], V. Jakumaitė[5], N. Kažukauskienė[6], V. Gelžinienė[7]

[1–7]Behavioral Medicine Institute, Lithuanian University of Health Sciences, Lithuania
E-mail: *[1]jbro@ktl.mii.lt, [2]ingad@ktl.mii.lt,[3]brigitav@hotmail.com, [4]mstaniute@ktl.mii.lt, [5]vilija@ktl.mii.lt, [6]nijolekazukauskiene@yahoo.com, [7]vaidagelziniene@yahoo.com*

Abstract. Exercise capacity is known to be an important prognostic factor in patients with cardiovascular disease, particularly after myocardial infarction (MI). Impaired exercise capacity may result from several mechanisms including residual ischemia, left ventricular dysfunction, impaired peripheral adaptation, reduced heart rate variability to exercise, inflammatory and others factors. The aim of the study was to evaluate the factors affecting improvement in exercise capacity in patients after MI during early short-term exercise – based rehabilitation program.

Keywords: exercise capacity, left ventricular function, heart rate variability, cardiac rehabilitation.

Introduction

Exercise capacity is known to be an important prognostic factor in patients with cardiovascular disease, particularly after myocardial infarction (MI). Impaired exercise capacity may result from several mechanisms including residual ischemia, left ventricular dysfunction, impaired peripheral adaptation, and reduced heart rate variability to exercise, inflammatory and others factors [1–6]. The aim of the study was to evaluate the factors affecting improvement in exercise capacity in patients after MI during early short-term exercise – based rehabilitation program.

Methods and Contingent

In cross-sectional study 211 patients take part with documented acute MI (75% men and 25% women, mean age 57±9 years), admitted for cardiac rehabilitation program. They were evaluated for demographic characteristics, clinical state, for symptoms of depression/anxiety and for standard echocardiography data. Exercise capacity (EC) was evaluated using symptom-limited bicycle ergometer test, calculated as total METs achieved at peak workload (PW). All patients underwent evaluation resting and exercise heart rate variability (HRV) via the HR monitoring system on-line to PC. Standard HRV patterns were analysed: the mean R-R interval (RR, ms), standard deviation of all R-R intervals (SDNN, ms), and the very low (VLF, ms), low (LF, ms) and high frequency (HF, ms) components of HRV spectrum during rest. On the basis of the rhythmogram (RR intervals), registered during bicycle ergometry, HR variability quantitative parameters from RR Poincare plots were analysed: HR average (RR), maximal and minimal HR (RRmax, RRmin), maximal HR response (DRRr) or reflex control level, maximal HR variability (DRRt) reflects tonic control level, total HR variability (σRR), the part of variability related to the respiration (V) – correlated with parasympathetic impact, and general HR variability (S) measured as the square of the plot – involving both tonic and reflex control components. EC and HRV data were evaluated twice – before and after rehabilitation program.

Results

After early rehabilitation program EC significantly increased from 3.6 ±1.0 till 4.0±1.1 METs ($p<.001$). Improvement in EC definite in 145 (69%), decrease in 24 (11%), and EC remain

unchanged – in 42 (20%) patients after MI. Growing in EC was about 30% (12.3±19.9%). Dynamic data of resting HRV (the time and frequency domain data) showed that variables after short-term exercise – based rehabilitation program did not changed reliably. Data of HR Poincare plots registered during repeatable exercise test had showed significant increase ($p<.05$) in total HR variability ($\sigma RR = 116.1 \pm 42.5$ vs. 125.5 ± 42.8 ms), lessen of the minimal HR value ($RRmin = 629.8 \pm 98.9$ vs. 607.6 ± 95.8 ms), as well as increase in maximal HR response ($DRRr = 454.2 \pm 145.6$ vs. 488.7 ± 145.8 ms), demonstrating improvement of chronotropic function as well as recovery of autonomic reflex control level. Left ventricular ejection fraction in the group was 47.7±7.8%. Three models of multivariate linear regression analysis (enter method) was performed to identify the independent predictors of basal EC, EC after rehabilitation and improvement in EC (stepwise) after adjusting for age, gender, heart failure, angina pectoris class, diabetes mellitus, anxiety/depression symptoms, echocardiography data and HR variability values at rest and during exercise test. Determinants of baseline EC (model $R2 = 0.68$) were gender ($\beta = –0.30$, $p = .001$), heart failure stages ($\beta = –0.35$, $p = .0001$), data of echocardiography ($\beta = –0.33$, $p = .007$) and maximal HR during PW ($\beta = –0.24$, $p = .006$). Determinants of EC after rehabilitation (model $R2 = 0.67$) remained gender, initial data of echocardiography, reducing of depression symptoms ($\beta = –0.18$, $p = .029$), exercisežrelated heart rate variability ($\beta = 0.65$, $p = .025$) and maximal HR during PW ($\beta = –0.24$, $p = .003$). The improvement in EC (model $R2 = 0.43$) was determined by baseline EC ($\beta = –0.69$, $p<.001$), heart failure stages ($\beta = –0.26$, $p = .019$), exercise-related HRV ($\beta = 0.85$, $p = .025$) and maximal HR during PW ($\beta = –0.25$, $p = .032$).

Conclusion

After short-term exercise-based rehabilitation program exercise capacity in patients after myocardial infarction is strongly related with gender, data of echocardiography, reduction symptoms of depression, exercise-related heart rate variability, and maximal heart rate achieved during peak workload. Improvement in exercise capacity is related with basal exercise capacity, heart failure stages, exercise-related heart rate variability and maximal heart rate during peak workload.

References

[1] **Monmeneu J.V., Chorro F.J., Bodi V., Sanchis J., Llacer A., Garsia-Civera R., Ruisz R., Sanjuan R., Burguera M., Lopez-Merino V.** Relationships between heart rate variability, functional capacity, and left ventricular function following myocardial infarction: an evaluation after one week and six months. Clin. Cardiol., 24, 2001, p. 313–320.

[2] **Iellamo F.** Neural mechanisms of cardiovascular regulation during exercise. Autonomic Neuroscience: Basic and Clinical, 90, 2001, p. 66–75.

[3] **Oya M., Itoh H., Kato K., Tanabe K., Murayama M.** Effects of exercise training on the recovery of the autonomic nervous system and exercise capacity after acute myocardial infarction. Jpn Circ J, 63, 1999, p. 843–848.

[4] **Specchia G., De Servi S., Scire A., Assandri J., Berzuini C., Angoli L.** *et al***.** Interaction between exercise training and ejection in predicting prognosis after a first myocardial infarction. Circulation, 94, 1996, p. 978–982.

[5] **Freitas P.D., Haida A., Bousquet M., Richard L., Mauriege P., Guiraud T.** Short-term impact of a 4-week intensive rehabilitation program on quality of life and anxiety-depression. Ann Phys Rehabil, 229, 2011, p. 1–12.

[6] **Egger E., Schmid J.P., Schmid R.W., Saner H., von Kanel R.** Depression and anxiety symptoms affect change in exercise capacity during cardiac rehabilitation. Eur J Cardiovasc Prev rehabil, Vol. 15, Issue 6, 2008, p. 704–8.

Comparison of the two noninvasive methods for assessment of liver fibrosis

Diana Aksionova[1], Eglė Audronytė[2], Ilona Savlan[3], Valentina Liakina[4]

[1, 2, 3, 4]Vilnius University Faculty of Medicine, Lithuania
[4]Vilnius Gediminas Technical University, Lithuania
E-mail: [1]*diana.aksionova@vu.lt,*[2]*egle.audronyte@vu.lt,* [3]*ilona.savlan@vu.lt,* [4]*valentina.liakina@santa.lt*

Abstract. Noninvasive liver fibrosis evaluation and monitoring during antiviral treatment would be very useful in clinical practice. For that purpose some easily calculated indices are used. APRI and FIB-4 indices are calculated using AST blood activity and platelets count. According to obtained data both indices are suitable for the evaluation of severe fibrosis in patients with chronic hepatitis C.

Keywords: hepatitis C, fibrosis, non-invasive markers of fibrosis, indices.

Introduction

The aim of this study was to evaluate differences in of basic blood count and routine clinical chemistry tests in chronic hepatitis C patients with mild and advanced fibrosis and validate non-invasive prognostic indices for the assessment of significant fibrosis.

Patients and methods

173 chronic hepatitis C or viral C cirrhosis patients (84 women, 89 men, mean age 39.6±11.7) were enrolled. Basic blood count, clinical chemistry tests and liver biopsy was performed for all patients. Fibrosis was graded using METAVIR scale. According to fibrosis score patients were divided into 2 groups: I – with mild fibrosis (METAVIR 0-I) and II – with advanced fibrosis (METAVIR II-IV).

The APRI (AST-to-platelet-Ratio-Index) was calculated by formula: **(AST/ULN)/platelets x 100**, where AST is asparagine transaminase and ULN is the upper limit of the normal range of this enzyme both expressed in international units/l (IU/L) [1, 2]. The FIB-4 score was calculated using Sterling's formula, as follows: **age [years] × AST [IU/L]/platelet count [expressed as platelets × 109/L] × (ALT1/2[IU/L])** [3, 4].

APRI and FIB-4 indices specificity and sensitivity in diagnosis of advanced fibrosis were evaluated by calculation of area under ROC curves. If the area was >0.7 we considered index suitable for diagnostic use. Differences in the routine blood and biochemical tests results between 2 groups of patients were evaluated using nonparametric Fisher and Chi-square tests, data were considered statistically significant if $p<0.05$.

Results

Statistically significant difference in platelet count, erythrocyte sedimentation rate and liver enzymes activity concentrations was found between 2 groups of patients (Table 1).

The area under ROC curves showed that both indices are suitable for detection of significant fibrosis: APRI – 0.811; FIB-4 – 0.740. The sensitivity and specificity for APRI index was 81.9% and 75% while for FIB-4 – 57.7% and 91,7%, respectively.

Table 1. Blood tests results of patients with different grade of liver fibrosis

Test	I gr.	II gr.	p
Lymphocytes (10^9/l)	7,6±2,3	6,9±1,9	0,64
Erythrocytes (10^{12}/l)	4,7±0,5	4,66±0,45	0,76
Platelets (10^9/l)	242±42	203±65	0,019
Erythrocytes sedimentation rate (mm/h)	6,1±6,0	14,3±12,6	0,046
Bilirubin (μmol/l)	21,1±17,9	13,9±8,9	0,44
Alanine-aminotransferase (IU/l)	64,6±15,5	120,5±69,6	<0,001
Asparagine-aminotransferase (IU/l)	38,3±18,4	74,3±50,8	<0,001
γ-glutamyl-transpeptidase (IU/l)	32,1±26,0	87,3±36,7	<0,001
Alkaline phosphatase (IU/l)	61,2±19,6	69,8±25,7	0,24

Conclusions

Statistically significant differences in basic blood count parameters and clinical chemistry tests were found between patients with mild and advanced fibrosis. APRI index is more reliable predictor of advanced fibrosis in chronic hepatitis C patients than FIB-4.

References

[1] **Jin W, Lin Z, Xin Y, Jiang X, Dong Q, Xuan S.** Diagnostic accuracy of the aspartate aminotransferase-to-platelet ratio index for the prediction of hepatitis B-related fibrosis: a leading meta-analysis. BMC Gastroenterology. 2012; 14: 12–14.

[2] **Castera L.** Noninvasive methods to assess liver disease in patients with hepatitis B or C. Gastroenterology. 2012; 142(6): 1293–1302.

[3] **Tamaki N, Kurosaki M, Tanaka K, Suzuki Y, Hoshioka Y, Kato T, Yasui Y, Hosokawa T, Ueda K, Tsuchiya K, Nakanishi H, Itakura J, Asahina Y, Izumi N.** Noninvasive estimation of fibrosis progression overtime using the FIB-4 index in chronic hepatitis C. J Viral Hepat. 2013 Jan; 20(1): 72–6.

[4] **Paunovic K, Stojanovic M, Dimitrijevic Z, Paunovic G, Djordjevic V, Konstantinovic L, Kostic S.** Indirect serum fibrosis markers in hepatitis C virus (HCV) infection. Med Arh. 2012; 66(4): 226–30.

Association between body composition, physical performance and physical functioning in coronary artery disease patients

Brigita Vaičiūnienė [1], Nijole Kažukauskienė [2], Elena Bovina[3], Julija Brožaitienė [4]

Lithuanian University of Health Sciences, Academy of Medicine, Institute of Behavioral Medicine, Lithuania
E-mail: *[1]brigita@ktl.mii.lt, [2]nijolekazukauskiene@yahoo.com, [3]elenbovina@yahoo.com, [4]jbro@ktl.mii.lt*

Keywords: body composition, physical performance, physical functioning, CAD.

Introduction

The population is aging, which is associated with an increased prevalence of people reporting physical limitations. Studies showed that 40% of individuals older than 65 years reported at least one limitation. Moreover, physical performance (PP) can predict disability, institutionalization, and death. Body composition has been found to be related to lower PP in elderly persons. It is known also, that obesity and waist-to-hip ratio are the risk factors in CAD patients.

The aim of this study was to investigate the relationships between body composition, physical performance and physical functioning in coronary artery disease patients (CAD) during cardiac rehabilitation program.

Methods and contingent

In this study 123 patients (93 (74.8%) men and 31 (25.2%) women, age mean 56.3±8.9 years) with coronary artery disease were evaluated during cardiac rehabilitation program. The majority of patients were NYHA functional class II (78.9%). Mean aerobic capacity – 4.24±1.04 MET.

Body composition was assessed using caliperiometry. We calculated lean and fat mass. A relative measure of body composition, the lean-to-fat ratio, was calculated by dividing lean mass (fat free mass, FFM) by fat mass (FM).

Body mass index (BMI) was determined from height and weight measured (weight in kilograms/height in meters^2). Waist-to-hip ratio (WHR) was calculated by dividing waist circumference by hip circumference. It shows central adiposity. The waist circumference was measured in the standing position from midway between the lowest rib and the iliac crest (at the smallest section of the waistline). The hip circumference was measured in the standing position from the plane of both major femoral trochanters (widest part of the gluteal region).

Physical performance domains (muscle strength, balance, muscle endurance, flexibility, and aerobic capacity) were indicated by some tests. Muscle strength was testing by handgrip test – dynamometry (kg). Participants performed the hand grip strength test three times for both hands, and the best score was used for analysis. Balance evaluated by one leg standing test with closed eyes. Participants were standing for 30s and were count mistakes. Endurance measured by calf muscle endurance test (times per minute). Flexibility was assessed by sit and reach test (cm), side bending tests (cm). Cardiovascular capacity (aerobic capacity) was estimated by symptom- limited bicycle ergometric test (MET kGm).

All participants filled in Short-Form 36 (SF-36) questionnaire measuring health related quality of life. The SF-36 consists of 8 subscales measuring physical and mental health. Scores for each subscale range from 0 to 100; higher scores indicate better health status. For this study,

only Physical functioning scale (10 items) of the 8 subscales of the SF-36 was analyzed. The physical functioning (PF) subscale was analyses because these items ask questions about walking, lifting, climbing, and bending showing mobility and physical functioning.

Results

Correlation between body composition and physical performance domains showed that fat free mass-to-fat mass ratio positively correlated with flexibility (waist bending to the right) (r = .23, p<.05), dynamometry of both hands, right hand (r = .47, p<.001), and left hand (r = .42, p<.001), muscle endurance (r = .25, p<.05) and cardiovascular capacity (r = .22, p<.05).

BMI was negatively correlated with patients flexibility (waist bending forward) (r = .25, p<.05), aerobic capacity (r = .30, p<.05). Physical functioning positively correlated with, flexibility: waist bending right (r = .26, p<.05) and left (r = .21, p<.05), muscle strength: dynamometry of right hand (r = .34, p<.000), left hand (r = .35, p<.000), muscle endurance (r = .23, p<.05) and free fat mass-to-fat mass ratio (r = .26, p<.05).

We used multivariate linear regression analyses to examine association of body composition with physical performance components, adjusted for age, gender, NYHA class.

We found that muscle strength was associated with BMI (β = .22, p<.05) and waist-to-hip ratio (β = .18, p<.05). Cardiovascular capacity was associated with NYHA (β = .35, p<.000). In another models analyzed association physical functioning (SF–36) with body composition and physical performance components, adjusted for age, gender, NYHA class. Physical functioning was associated with BMI (β = –.17, p<.05) and central adiposity (waist to hip ratio) (β = –.29, p< .05).

Conclusions

In CAD patients, undergoing rehabilitation, fat free mass, and body mass index is related to physical performance domain and physical functioning is associated to central adiposity and body mass index. Physical functioning was better for men with less central adiposity. Our result may suggest that weight management intervention would be helpful to maintain and improve physical performance and physical functioning during rehabilitation.

References

[1] **Haight T, Tager I, Sternfeld B, Satariano W, van der Laan M**. Effects of body composition and leisure-time physical activity on transitions in physical functioning in the elderly. Am J Epidemiol 2005, 162: 607–617.

[2] **Sternfeld B, Ngo L, Satariano WA, Tager IB**. Associations of body composition with physical performance and self-reported functional limitation in elderly men and women. Am J Epidemiol 2002, 156: 110–121.

[3] **Tager IB, Haight T, Sternfeld B, Yu Z, van Der Laan M**. Effects of physical activity and body composition on functional limitation in the elderly: application of the marginal structural model. Epidemiology 2004, 15: 479–493.

[4] Body Mass, Fat-Free Body Mass, and Prognosis in Patients with Chronic Obstructive Pulmonary Disease from a Random Population Sample. Findings from the Copenhagen City Heart Study. Am J Respir Crit Care Med, 2006 Vol 173, p. 79–83.

Approximate Closed-Form Solution of the Synovial Pressure Field in the Human Ankle Joint with non-Newtonian Lubricant and Deformable Cartilage Layer

Alessandro Ruggiero [1], Roberto D'amato [2], Emilio Gómez [3], Sergej Hloch [4]

[1]Department of Industrial Engineering, University of Salerno. Italy
[2–3]Departamento de Mecánica Industrial -Universidad Politécnica de Madrid, Madrid. Spain
[4]Faculty of Manufacturing Technologies TUKE with a seat in Prešov, Slovak Republic
E-mail: [1]*ruggiero@unisa.it,* [2]*r.damato@upm.es,* [3]*emilio.gomez@upm.es,* [4]*sergej.hloch@tuke.sk*

Keywords: Hydrodynamic Lubrication, Analytical Model, Biotribology, Ankle Joint.

Introduction

The study of the synovial joints mechanism has recently become an active area of scientific research. The human joint is a dynamically loaded bearing [1, 2, 3] which employs articular cartilage as the bearing and synovial fluid as the lubricant. Once a fluid film is generated, squeeze-film action is capable of providing considerable protection to the cartilage surface. Such joints have a low friction coefficient and negligible wear. However, when the natural joints fail to function properly, a possible remedy is the replacement of these by artificial joints.

During joint motion or when the cartilage is compressed, fluid content of the cartilage flows through the outermost layer of cartilage. The fluid flows back the moment the motion or compression is ceased. The moving fluid reduces friction and nourishes the blood vessel and cartilage. The human ankle joint can be simply taken as cylindrical [4], enabling rotation in the sagittal plane only. The joint is represented by two rigid circular cylinders in the inner contact (a cylinder encased in a cylindrical cavity), coated with thin layers of cartilage. The coupling model is assumed by two infinite rigid circular cylinders (subchondral bone) in the internal contact (a cylinder encased in a cylindrical cavity), covered with thin layer (articular cartilage) of uniform thickness; the lower (talar) articular surface is supposed stationary while the upper (tibial) surface is assumed to have pure squeeze motion $\dot{\varepsilon}(t)$ (Fig. 1).

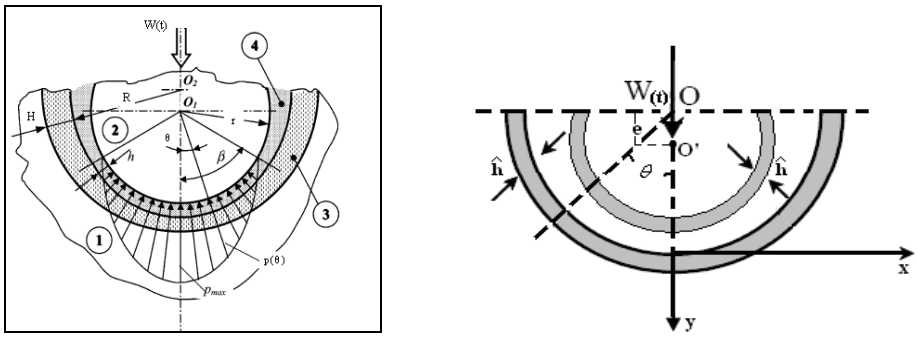

Fig. 1. a) Geometry of ankle joint. (1), (2)-Bone, (3)-cartilage layer, (4)-synovial fluid;
b) Human ankle joint equivalent bearing

The long chain polysaccharide hyaluronic acid molecules present in the synovial fluid give us the motivation for modeling of the synovial fluid as a Stokes [3] couple-stress fluid.

Making the usual assumptions of hydrodynamic lubrication applicable to thin films [6], and considering the flow of a viscous fluid in a porous matrix governed by modified Darcy's law [3],

the modified Reynolds equation, considering the nomenclature in Table 1, written in a non-dimensional form is:

$$\frac{\partial}{\partial\theta}\left\{\frac{\partial p^*}{\partial\theta}\left[f^*\left(h^*,l^*\right)+\frac{12\Phi^* H^*}{(1-\alpha)}\right]\right\}=12\cos(\theta). \tag{1}$$

As regards the determination of the thickness of the fluid film can be estimated that the same can be assessed as the sum of a component linked to the geometry of the system and another related to the elastic deformation of the thin coating cartilage, namely:

$$h=h_g+h_e. \tag{2}$$

Results and Conclusions

This approach gives the advantage to obtain an analytical expression of the synovial pressure field and of the non-stationary fluid film force acting in the synovial joint during the squeeze motion in terms of couple-stress parameter, film thickness, porosity and soft deformation parameters.

The calculated values for the pressure field and for the approximate fluid film force have been compared with those in [1, 2, 3] and they show a good agreement.

Table 1. Main nomenclature

e, ε	Eccentricity, Eccentricity ratio	h	Synovial film thickness	p, p^*	Pressure in the film region, Dimensionless pressure
R	Effective radius curvature of the contact	H	Porous layer thickness	θ	Circumferential coordinate
E	Young's modulus of the cartilage matrix	l, l^*	Couple stress parameter, dimensionless couple stress parameter	ϕ	Permeability of the cartilage matrix
L, L^*	Equivalent bearing length, Dimensionless bearing length	f_r	Synovial fluid film force	μ	Viscosity of synovial fluid

References

[1] **Walicki E., Walika A.** Mathematical modelling of some biological bearings. Smart Mater. Struct. 9 p. 280–283, (2000).

[2] **Ruggiero A., Gòmez E., D'Amato R.** Approximate Analytical Model for the Squeeze-Film Lubrication of the Human Ankle Joint with Synovial Fluid Filtrated by Articular Cartilage. TRIBOLOGY LETTERS, vol. Volume 41– N.2, p. 337–343, ISSN: 1023-8883, doi:10.1007/s11249-010-9710-5 (2010).

[3] **Ruggiero A., Gòmez E., D'Amato R.** Approximate closed-form solution of the synovial fluid film force in the human ankle joint with non-Newtonian lubricant. TRIBOLOGY INTERNATIONAL. Vol 57, p. 156–161, 2013, ISSN 0301-679X.

[4] **Walicki, E. and Walicka, A**. Inertia and couple-stress effects on squeeze-film characteristics with reference to biological bearings. Tribotest J., 2002, 8(3), 195–203.

[5] **Bujurke, N. M., Bhavi, S. G., and Naduvinamani, N. B.** The effect of couple stresses in squeeze film poroelastic bearings with special reference to synovial joints. IMA J. Math. Appl.Med. Biol., 1990, 7, 231–243.

[6] **Stokes,V. K.** Couple stresses in fluids. Phys. Fluids, 1966, 9, 1709.

[7] **Naduvinamani NB, Hiremath PS, Gurubasavaraj G.** Static and dynamic behaviour of squeeze film lubrication of narrow porous journal bearings with couple-stress fluid. Proc. Instn. Mech. Engrs, Part J 2001; 215: 45–62.

[8] **Lin J.-R. (1996),** Couple-stress effect on the squeeze film characteristics of hemispherical bearings with reference to synovial joints. – Appl. Mech. Eng., vol. 1, No. 2, p. 317–332.

[9] **Ruggiero A., Senatore A.** Approximate closed-form solution for the dynamical analysis of short bearings with couple stress fluid. Lubrication Science, vol. 19, p. 247–267, doi:10.1002/ls.47.

On the Roughness Measurement of the Knee Femoral Components

Saverio Affatato [1], Laura Grillini[1], Stefano Falcioni[1], Alessandro Ruggiero[2]

[1] Medical Technology Laboratory, Rizzoli Orthopaedic Intitute, Bologna, Italy
[2] Department of Industrial Engineering, University of Salerno, Italy
E-mail: [1]*affatato@tecno.ior.it,* [2]*ruggiero@unisa.it*

Keywords: surface profile, wear, *in vitro* experiments, artificial knee joints.

Introduction

A total knee replacements (TRK) currently implanted is formed by a metallic femoral component and a tibial component formed by a metallic support plate and a polyethylene insert [1]. Aseptic loosening of the femoral, or tibial, or patellar component (or a combination), and wear phenomena are among the most common causes of failure of TKR [2–3–4–9]. Moreover, abnormal stresses at the joint interface may increase polyethylene wear and as a consequence cause the failure of the implant [5]. The finishing surface of the metal components is a very important factor to minimize the polyethylene wear rate and then the progressive production of metal and plastic debris [5–6–10]; a high surface roughness of the metallic component, due to inaccurate machining or to the damage produced by a third-body, can dramatically increase the wear rate [7]. There is a large consensus in the literature on the role of surface roughness on the volumetric wear rates, for that concern the hip prostheses, while no report are available for the knee prostheses [6–8–11]. The purpose of this study is to develop a protocol for the roughness characterization of TKR metal components, considering a limited number of points on every surface.

Materials and Methods

Six mobile TKR divided into different sizes (three TKR of size 2 and three TKR of size 6) were tested on a knee joint simulator to compare the wear behaviour of each groups. After 2×10^6 cycles the weight lost by the polyethylene inserts was measured with gravimetric method and the surface roughness of the metallic components was assessed in terms of average surface roughness R_a and skewness R_{sk}.

The measurements of the surface profile were performed on all metal components using a dimensional contact SRM machine (Hommel Tester T8000, Hommel Werke, Germany) equipped with a diamond stylus tip of radius 0.020 mm and a M1 digital filter assigned according to DIN 4777 part 1. The machine provides various measuring ranges (absolute), from ±8 to ±8000 mm with a resolution from 1 to 1000 nm respectively. Immediately before measurement, the specimens were wiped with acetone. Sampling lengths were taken using a cut-off of 0.25 mm. The choice of the cut-off is of fundamental importance to determine a representative parameter, in order to estimate the correct roughness measurements as recommended by the aforementioned ISO normative. The system is computer-controlled and all surface parameters were recorded for each measurement. The software provided a dimensional and topographic view of the head surface and characterized it in terms of surface profile parameters. Roughness measurement involved 29 points on each femoral condyle and about 25 points on each metal tibial plate. Inspection of the articulating surfaces with the unaided eye revealed that wear occurred primarily on the distal region of the condyles where the femoral component articulated against the plateau of UHMWPE tibial component, so for surface roughness analysis was identified an area which covered the majority of the worn area on each condyle. Having analyzed implants of two different sizes (size 2 and size 6) the measures of the areas are different and proportionate to the size of the implant, so we have an area of 30.7 mm × 25 mm for the size 6 and an area of 23 mm × 20.3 mm for the size 2.

The points on which to perform the measurements within the considered area have been identified by the intersection between horizontal planes and segments of the main surface. Within the entire surface of the analyzed tibial plate the areas have been identified.

Results

The results obtained from roughness measurements were statistically analyzed in order to assess their significance and then see if the proposed protocol is designed to provide a proper surface characterization. The analysis of the results was performed by ANOVA and t test. In both cases the tests return a value, "P value", according to which the difference between groups is significant or not. The groups appear to have no significant difference if the "P value" is greater than 0.05, otherwise the test highlights the differences between the groups and, specifically, the number of measurements taken is insufficient.

The data collected has shown an increased roughness upon wear testing for both the investigated TKR sizes. As shown in the tables 1–2–3–4, almost all of the groups analyzed, no statistical differences (ANOVA and t-test) were observed between the groups for both the parameters Ra and Rsk. The analysis attest that the method used to derive the positions of measurement is valid for the femoral and tibial components obtained from in vitro tests.

The work carried out has confirmed the importance of the parameter Ra in the description of the surface of the femoral components, but at the same time showed the validity of the parameter Rsk, which in some cases result is a better descriptor roughness for the areas studied which integration of information collected from Ra, in fact, in many cases the surface of the metal components assumes negative values of asymmetry, indicating diminishing peaks. The study has tried to draw a line guide for further investigations to develop a protocol that allows users to make measurements of the roughness parameters on the metal components of knee prostheses.

Acknowledgements

The author gratefully acknowledges the experimental activity performed by Mr. Jonathan De Mattia during his Bachelor Degree Thesis developed in cooperation between the Department of Industrial Engineering of the University of Salerno and the Medical Technology Laboratory of the Rizzoli Orthopaedic Intitute (Bologna Italy).

References

[1] **Peter A. Revell** Joint replacement technology. USA: 2008.

[2] **D. Zhao, W. G. Sawyer, B. J. Fregly** Computational Wear Prediction of UHMWPE in Knee Replacements. Journal of ASTM International. 2006.

[3] **H. A. McKellop, I. C.** Clarke Degradation and wear of UHMWPE, corrosion and degradation of implant materials. Philadelphia: 1985.

[4] **H.C. Amstutz, P. Campbell, N. Kossovsky, I.C. Clarke** Mechanism and clinical significance of wear debris-induced osteolysis. Clin. Orth. Res., Vol. 276, 1992.

[5] **McGloughlin, Kavanagh** Wear of ultra-high molecular weight polyethylene (UHMWPE) in total knee prostheses: A review of key influences. 2000.

[6] **Lloyd, A. I.** and **Noel, R. E.** The effect of counterface surface roughness on the wear of UHMWPE in water and oil-in-water emulsion. *Tribology Int.*, 1988.

[7] **Haley, J. L., Ingham, E., Stone, M.,Wrobleski, B. M.,** and **Fisher, J.** Ultra-high molecular weight poly ethylene wear derbris generated *in vivo* and in laboratory tests; the influence of counterface roughness. Proc. Instn Mech. Engrs, Part H: J. Engineering *in Medicine*, 1996.

[8] **Affatato *et al*.** The predictive power of surface profile parameters on the amount of wear measured in vitro on metal on polyethylene artificial hip joints. 2005.

[9] **Lewis G.** Polyethylene wear in total hip and knee arthroplasties. J Biomed Mater Res 1997.

[10] **Revell PA, Weightman B, Freeman MAR, Roberts BV.** The production and biology of polyethylene wear debris. Arch Orth Traum Surg, 1978.

[11] **Weightman B, Light D.** The effect of the surface finish of alumina and stainless steel on the wear rate of UHMWPE. Biomater, 1986.

An Analytical Expression for the D.I.P. – P.I.P. Flexion Interdependence of the Human Finger

K.J. van Zwieten[1], K.P. Schmidt[2], G.J. Bex[3], P.L. Lippens[4], W. Duyvendak[5]

[1, 2, 3, 4]University of Hasselt, Belgium
[5]Jessa Hospital Hasselt, Belgium
E-mail: [1]*koosjaap.vanzwieten@uhasselt.be,* [2]*klaus.schmidt@uhasselt.be,* [3]*geertjan.bex@uhasselt.be,* [4]*pl.lippens@skynet.be,* [5]*wim.duyvendak@jessazh.be*

Keywords: distal interphalangeal joint, proximal interphalangeal joint, kinematical model of finger flexion, D.I.P. – P.I.P. flexion interdependence, intrinsic-minus fingers.

Background

Some clinicians feel the need to investigate the correlation between the flexion ranges of the different finger joints for a clear distinction between a healthy and a pathological finger. When investigating the interrelation of quantities in different (e.g. healthy and pathological) cases, it is often more instructing, not to compare the direct change of the involved quantities, but to compare their rate of change, expressed by the first order derivative. Empirical evidence shows that a strong correlation exists between the flexion angles of the distal interphalangeal joint (D.I.P.), and the proximal interphalangeal joint (P.I.P.) of the human finger. The aim of the study therefore is to find an analytical expression for this correlation, from where the first derivative may be calculated. A line defined by the straight dorsum of the middle phalanx gives the reference from where the flexion angles θ (P.I.P. flexion) and φ (D.I.P. flexion) are measured. This is shown in a lateral view in Fig. 1. Several authors report the measured functional dependence of the D.I.P. angle on P.I.P. flexion [1, 2, 3, 4]. They also state that the interdependence of D.I.P. and P.I.P. flexion is different for healthy individuals and patients suffering from various pathologies. Examples of such pathologies are: peripheral neuropathies and joint diseases such as rheumatoid arthritis (RA) and osteoarthritis (OA) [3, 4].

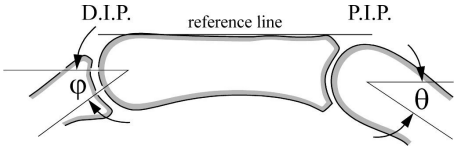

Fig. 1. Definition of D.I.P. – P.I.P. flexion angles. Diagram based on a lateral view of the human finger; left: distal; right: proximal

Method

We developed a kinematical model expressing analytically the D.I.P. – P.I.P. angle correlation as $\varphi = f(\theta)$. In order to get numerical expressions, the model was applied to two experimental data sets, one set for a normal finger, the other for a pathological finger. The anatomical model parameters, as far as they are P.I.P. angle dependent, are, after adapting them empirically to best fit a given data set, expressed by a least squares fit polynomial in the P.I.P. angle θ and inserted into the model expression. We thus obtained an overall analytical formula fitting the given data sets.

Findings

We were able to model the D.I.P. – P.I.P. angle interdependence and to describe it by means of an analytical form. This function allows for any P.I.P. angle to calculate the corresponding D.I.P. angle. After first order differentiation of the analytical expression with respect to the P.I.P. angle, the model also shows the rate of change of the D.I.P. flexion. The function and its first order derivative are applied to two sets of data, for a healthy and a pathological situation respectively. Fig. 2 shows the fit of the healthy state, Fig. 3 the fit of the pathological state, in this case a peripheral neuropathy of the ulnar nerve at the elbow leading to "intrinsic-minus fingers", also known as "clawing fingers" [5, 6].

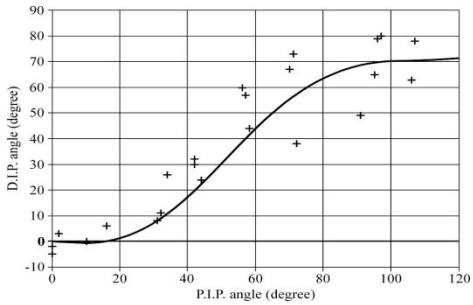

Fig. 2. Experimental data (crosses) and analytical fit (line) of D.I.P. – P.I.P. flexion angles for a healthy finger

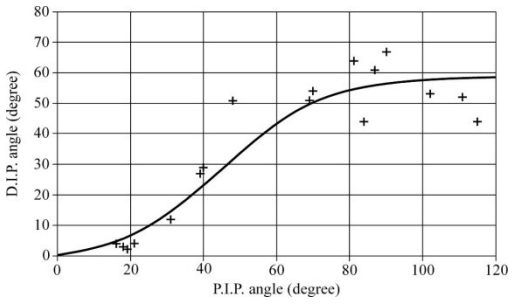

Fig. 3. Experimental data (crosses) and analytical fit (line) of D.I.P. – P.I.P. flexion angles for a pathological finger

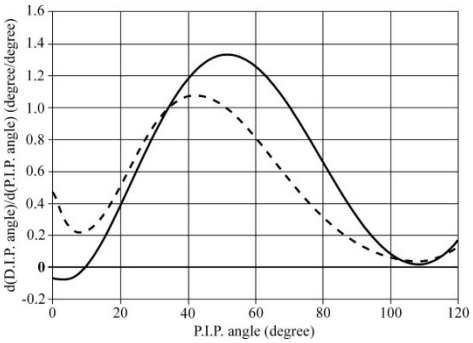

Fig. 4. Calculated derivatives of the analytical fits of the D.I.P. – P.I.P. flexion angles for a healthy (solid line) and a pathological (dotted line) finger

Interpretation

Especially the calculation and visualisation of the rate of change of the D.I.P. flexion versus P.I.P. flexion (Fig. 4) provides an additional and more precise discriminatory tool between normal and pathological states, such as a peripheral neuropathy. As Fig. 4 shows, this rate of change is different for a healthy and a pathological finger. In the pathological finger the maximum of D.I.P. flexion per degree of P.I.P. flexion is lower than in the normal finger. Further on, for the pathological finger the maximum of D.I.P. flexion lies about 10 degrees P.I.P. angle lower than the maximum in the normal finger. Not only reaches the maximum of flexion in the pathological finger only 80% of the maximal flexion of a normal finger, the ability to flex the D.I.P. joint more, declines faster than in a normal finger when going to higher P.I.P. values. In other words, in the intrinsic-minus finger, D.I.P. flexion "runs ahead" of P.I.P. flexion. This

phenomenon may also be held responsible for the kinematic aspects of the intrinsic-minus finger, also called the “claw-finger deformity” [6].

Conclusion

Especially the visualisation of the rate of change of the D.I.P. flexion versus P.I.P. flexion provides an additional and clear-cut discriminatory tool between normal and pathological states of the finger.

References

[1] **Hahn P., Krimmer H., Hradetzky A., Lanz U.** Quantitative Analysis of the Linkage between the Interphalangeal Joints of the Index Finger. An in vivo study. Journal of Hand Surgery (British and European Volume), Vol. 20B, Issue 5, 1995, p. 696–699.

[2] **Holguín P. H., Rico Á. A., Gómez L. P., Munuera L. M.** The Coordinate Movement of the Interphalangeal Joints: A Cinematic Study. Clinical Orthopaedics and Related Research, Vol. 362, 1999, p. 117–124.

[3] **Van Zwieten K. J., Lippens P. L., Gelan J., Adriaensens P., Schmidt K. P., Thywissen C., Duyvendak W.** Coordination of interphalangeal flexion in the human finger. Journal of Hand Surgery (British and European Volume), Vol. 33, Issue 1, 2008, p. 170–171.

[4] **Leijnse J. N. A. L., Quesada P. M., Spoor C. W.** Kinematic evaluation of the finger’s interphalangeal joints coupling mechanism – variability, flexion-extension differences, triggers, locking swanneck deformities, anthropometric correlations. Journal of Biomechanics, Vol. 43, 2010, p. 2381–2393.

[5] **McNamara B.** The Ulnar nerve. Advances in Clinical Neuroscience and Rehabilitation, Vol. 3, Issue 2, 2003, p. 25–26.

[6] **Srinivasan H.** Movement patterns of intrinsic minus fingers. Role of intrinsic and extrinsic muscles in finger posture control. Annals of the Royal College of Surgeons of England, Vol. 59, 1977, p. 33–38.

On calculation of the human circumferential measures using wide angle lens photogrammetry system

Dmitrijs Celinskis[1], **Alexei Katashev**[2], **Vineta Zemite**[3]

[1–3] Institute of Biomedical Engineering and Nanotechnologies, Riga Technical University, Latvia
E-mail: [1]*dmitrijscelinskis@yahoo.co.uk,* [2]*katashev@latnet.lv,* [3]*vzemite@latnet.lv*

Abstract. To obtain circumferential measure from two photogrammetric images, one have to approximate cross-section of the body part by some parametric curve. In the present paper, different ellipse – like approximations are considered with the aim to minimize difference between results of the direct and photogrammetric measurements.

Keywords: anthropometrics measurements, photogrammetry**.**

Introduction

Measurements of the human body geometric parameters often become the important part of the patient screening programs. In particular, such measurements as height (recalculated to the body mass index), waist ant tight circumference are the first indicators of the overweight; the latter is an important risk factor. For modern screening applications, that is a tendency to replace traditional measurement tapes, rulers and calipers with computer-based devices; this allow to "unite" various diagnostic modalities in a single screening complex [1].

There are number of techniques, proposed for the measurement of the anthropometrics parameters; examples include rather expensive 3D scanners, stereophotography, marker-based systems etc. Photogrammetry, although requires just single camera and simple calibration object still demonstrates reasonable accuracy in evaluation of posture via linear or angular measurements [2]. Besides, for circumferential measurements, such as waist, hips etc, the accuracy of the measurement, based on two person's images, say lateral and frontal, depends on the shape, used to replace real body cross section [3].

The goal of the present research is to find approximation of the human cross-section that could minimize the inaccuracy of the photogrammetric measurements of the waist and hip circumference.

Method and results

Waist and hip circumferences of the twenty one (21) young volunteers, born 1991–1993, was measured by means of the flexible measuring tape. Further, subjects was positioned on the square platform (side 50 cm) with the cross, marked at the center and used for further image calibration. Frontal and lateral images were obtained by means of wide lens camera (focal length 2.3 mm), placed 2 m from the center of the platform and at the height of 1.5 m. Camera lens distortion was corrected, following [4].

Subject's cross-sections was approximated by ellipse-like lines:

$$y = \pm b\left(1 - \left(\frac{x}{a}\right)^2\right)^{1/2} \text{ – ellipse.} \tag{1}$$

$$y = \pm b\left(1 - \left(\frac{x}{a}\right)^3\right)^{1/3} \text{ – cubic ellipse.} \tag{2}$$

$$y = +b\left(1 - \left(\frac{x}{a}\right)^2\right)^{1/2}, y = -b\left(1 - \left(\frac{x}{a}\right)^3\right)^{1/3} \text{ – combined ellipse,} \tag{3}$$

where a and b are the semi-axes of the curve.

Semi-axes a and b were measured from the patient image for the waist and hip level cross-sections. The circumference of the corresponding cross-section was calculates by numerical integration of the Eqs. (1)–(3). The correlation between circumferences, measured by the tape and calculated form image measurements, are presented at the Fig. 1

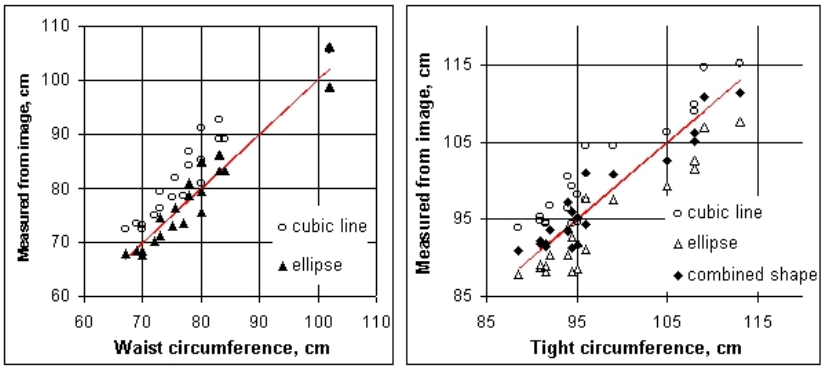

Fig. 1. Correlation between circumferential measures made "in nature" and from image: waist – left, tights –right

When the waist circumference is approximated by ellipse (Eq. 1), the difference between the photogrammetric and natural measurements of the waist was smallest and does not exceeded ±5.0 cm (P = 0.95). For the hip circumference, the best result was obtained for approximation 3, where the front side of the body is approximated by elliptic line (1), but rear side – by third order line (2): the above difference does not exceeded ±4.5 cm (P = 0.95).

Conclusions

With the proper selection of the approximation curve, circumferences measurements, made by photogrammetric method, demonstrates reasonable agreement with the "natural "data.

Acknowledgements

This work has been carried out in the framework of the European Regional Development Fund Project "Mobile Telemedicine Screening Complex", agreement Nr. 2011/ 0007/ 2DP/ 2.1.1.1.0/ 10/ APIA/ VIAA/ 008

References

[1] **Markovitch Z., Lauznis J., Balodis G., Katashev A., Markovitcha I.** Development of new mobile telemedicine screening complex. IFMBE Proceedings, vol. 38, 2013, IFMBE, p. 31–34.

[2] **Ferreira, E. A., Duarte M., Maldonado E. P., Bersanetti A. A., Marques A. P.** Quantitative assessment of postural alignment in young adults based on photographs of anterior, posterior, and lateral views," Journal of Manipulative and Physiological Therapeutics, vol. 34, no. 6, Jul. 2011, p. 371–380.

[3] **Chi-Yuen Hung P., Witana C.P., Goonetilleke R.S.** Anthropometric measurements from photographic images. In: Work with Computing Systems, Khalid H.M., Helander M.G., Yeo A.W. (Eds.), Kuala Lumpur: Damai Sciences, 2004, p. 764 – 769.

[4] **Celinskis D., Katashev A.** On criteria for wide-angle lens distortion correction for photogrammetric applications. IFMBE Proceedings, vol. 38 IFMBE, 2013, p. 153–158.

Influence of high heels on biomechanical parameters of the human gait

Vytautas Grigas[1], **Kristina Kazlauskienė**[2], **Danguole Satkunskienė**[3], **Aurelija Zdanytė**[4]

[1, 2, 3] Kaunas University of Technology, A. Mickeviciaus 37, 44244 Kaunas, Lithuania
E-mail: [1]*vytautas.grigas@ktu.lt,* [2]*kristina.kazlauskiene@ktu.lt,* [3]*danguole.satkunskiene@ktu.lt,* [4]*aurelija.zdanyte@stud.ktu.lt*

Abstract. The influence of the heel size on the kinematical parameters of human gait and the muscles activity is the topic of the research covered by this paper. The knee joint angle and electrical activity of the four muscles of human leg measured when walking on the treadmill with different speed on shoes hawing different height heel are analyzed.

Keywords: gait analysis, heel size, knee joint angle, muscles electrical activity.

Introduction

The feet is in continuous interaction with a shoe sole during walking, and the influence of the shoe heel, heightening the foot heel above the metatarsal heads, onto the gait biomechanical parameters is unquestioned [1]. When walking on a high heel shoes the whole posture is affected: the larger spine deflection appears, the center of mass displaces forward, so the maintenance of equilibrium is more difficult, the foot is deformed and foot pain arises [2]. A lot of the researches are carried out in this field during which a lot of high heel gait biomechanical parameters are investigated, but in most cases the muscles activity or motion kinematics is examined separately and in most cases the foot and ankle are in the focus [1–4].

The knee joint angle and electrical activity of the four muscles of human leg when walking on the treadmill with different speed on shoes hawing different height heel are the aim of the research described in this paper.

Investigation of the influence of high heels on human gait

To evaluate the influence of the heel height on the gait biomechanical parameters the experimental research of the human gait when walking on a treadmill with two different speeds (3,2 km/h and 4,2 km/h) wearing shoes with low (20 mm), middle (50 mm) and high (90 mm) heels, was carried out (one 22 years old female, height 165 cm, weight 48 kg). The variation of the knee joint angle was measured together with a four muscles of human leg electrical activity by means of electromyograph Myotrace-400 (Noraxon, USA) by using appropriate sensors (goniometer and EMG sensors). The measurement data were transmitted to a PC via Bluetooth and processed by MR-XP 1.07 MT404_Clinical Application Protocol software (the EMG signal has been divided into periods corresponding separate steps and filtered). Reliability of results has been checked by using SPSS Statistics software (statistical significance level $p<0,05$).

To evaluate the effect of a height of a shoe heel on the variation of knee joint angle the one cycle of total 20 measured for every regime of gait (heel height, speed of walking etc.) is extracted and the phases of motion are segregated. It can be seen that the largest amplitude is obtained for knee flection and extension phases during leg displacement. The dependencies of the knee joint angle amplitude in for different phases of the gait cycle on the heel height when walking on the treadmill with 3,2 km/h speed is shown on Fig. 1, a.

In the first half of cycle (amortization and take-off phases) the high heels (90 mm) leads to increment of the knee joint angle amplitude, and in the second half (knee flection and extension phases during leg displacement phase) – to the reduction. The 50 mm heel height seems to be optimal with regard to the knee joint angle, because in this case the gait is smoothest. The

change of knee joint angle amplitudes when walking with increased (4,2 km/h) speed (the reduction of duration of the gait cycle leads to decrement of joint angle amplitude in flection and extension phases) seems to be inconsiderable.

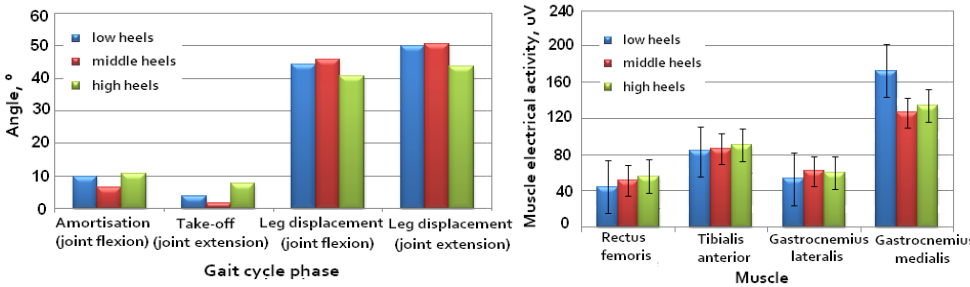

a b

Fig. 1. Dependencies of the gait biomechanical parameters on shoe heel height when walking with the 3,2 km/h speed: a – knee joint angle amplitude; b – muscles electric activity

To evaluate the effect of heel height on a leg muscles the electrical activity of Rectus femoris, Tibialis anterior, Gastrocnemius lateralis and Gastrocnemius medialis was measured by using Myotrace-400 with non-invasive, surface EMG sensors (having area 30–100 mm^2), sticked on the skin at the abdomen of the corresponding muscle. The gait regimes (heel heights, speed of walking) were the same as for knee joint angle measurements.

It was obtained, that when walking with a 3,2 km/h speed the electrical activity of Rectus femoris and Tibialis anterior grows with increment of the heel height (from the 42 to 56 μV and from the 82 to 92 μV correspondingly, see Fig. 1, b). That means that with a higher heel the more neurons are active in these muscles, because the larger force should be generated: for Rectus femoris – when straightening shin and flexing thigh, and for Tibialis anterior – when straightening feet. Such activation of neurons causes more intensive tiredness of muscles in comparison with walking on low or middle height heels shoes. The specific activity of Gastrocnemius medialis is also clearly seen: it is almost twice larger than for other muscles: the 172 μV for low heel (20 mm) shoes, 134 μV – for high heel (90 mm) and the lowest – 126 μV – for middle height (50 mm) heels shoes. The increment of walking speed leads to even larger difference in various muscles electrical activity.

Conclusion

The experimental research of the influence of heel height on the biomechanics of gait has confirmed the general negative effect of the high heels, however the influence of the heel height on the knee joint amplitude differs depending on the phase of joint movement (the 50 mm heel height is optimal during initial phases). The electrical activity of muscles unambiguously rises with increasing heel height, and increment of the speed of walking leads to higher activity of muscles and hereby – their tiredness.

References

[1] **Hansen A., Childress D.** Effects of shoe heel height on biologic roll-over characteristics during walking. J Rehabil Res Dev 2004; 41: 547–554.

[2] **Amit Gefen, M. Megido-Ravid, Y. Itzchak, M. Arcan.** Analysis of muscular fatigue and foot stability during highheeled gait, Gait and Posture, ISSN : 2230-9543 IJECT Vol. 3, 2002

[3] **Ásdís Árnadóttir, Inga Hrund Kjartansdóttir, Sigríður Katrín Magnúsdóttir.** Lower limb muscle activity. Electromyographic measurements of walking in high-heeled shoes compared to walking in trainers, 2011, http://skemman.is/handle/1946/9123

[4] **Sung-woo Park and Kunwoo Lee.** Simulation of biomechanical influence of high heels heels on musculoskeletal system of foot and ankle, in Proceedings of ISB2009, Cape Town, South Africa, Jul., 2009.

Research of the force characteristics of sports and rehabilitation exercise machines loading units

Aurelijus Domeika[1], **Vytautas Grigas**[2], **Anatolijus Šulginas**[3]

[1, 2, 3] Kaunas University of Technology, A. Mickevičiaus g. 37, 44244 Kaunas, Lithuania
E-mail: [1] *aurelijus.domeika@ktu.lt,* [2] *vytautas.grigas@ktu.lt,* [3] *anatolijus.sulginas@ktu.lt*

Abstract. The aim of this research was to examine the characteristics of resistance force (force dependencies on piston displacement) generated by linear hydraulic cylinder type loading units of exercisers acting in different regimes (resistance level and piston velocities). Experimental research of six devices has been performed by means of universal computerized material properties testing machine. The research showed that hydraulic cylinder type loading units of exercise machines generate quite uneven resistance force: depending on acting regime the variation of resistance force reach up to 30% of steady force.

Keywords: hydraulic cylinder, exercise machines, resistance force, piston velocity.

Introduction

Recently hydraulic cylinder type resistance devices are used extensively in exercise machines [1]. The resistance force in these devices is obtained by forcing viscous liquid through small cross-section channels [2]. When the athlete is moving the HC piston, liquid flows from one chamber of the cylinder to another through the channels made in the piston or in the ends of the cylinder, thus hydrodynamic resistance is directly dependent on the piston speed, the diameter of the piston (area) and the viscosity of the liquid [3]. This method of resistance is widely used in sports and rehabilitation exercise machines, whereas the hydraulic resistance load adapts to the natural muscle strength and allows achieving the full muscle load during the entire cycle [4]. Such loading units, practically not requiring maintenance, are widely used in steppers, rowing machines, selectors of different muscles groups and universal force exercise machines [4]. Some of them are supplied with mechanism for setting different level of resistance (by rotating ring controlling the cross-section of the channels connecting the chambers of cylinder or simply by adjusting the arms connecting cylinder to exerciser).

The aim of this research was to examine the characteristics of resistance force (force dependencies on piston displacement) generated by linear hydro-cylinder type loading units of exercisers acting in different regimes.

Force characteristics of hydraulic cylinder type loading units

Hydraulic cylinders of six exercise machines were investigated: lever type rowing (sculling) simulators (Nr. 1, 2 and 3, adjustable force) and steppers (Nr. 4, 5 and 6). Performance of hydraulic cylinders has been measured experimentally by using a universal computerized material properties testing machine "Tinius Olsen H25KT". The change of resistance force was measured at different piston velocities (60, 300, 600, 900 mm/min) and different resistance levels (I, IV, VIII, XII), repeating each test three times at constant 20 ºC temperature.

It was obtained that force characteristics of all adjustable HC obviously differ both qualitatively and quantitatively for different exercisers (Figs 1, a and 2) and are quite uneven in the beginning of stroke while the force characteristics of stepper's cylinders are smoother (Fig. 1, b). Fig. 2 shows the characteristics of resisting force generated by HC of rowing machines Nr. 1 and Nr. 2 at different resistance levels (velocity of piston 900 mm/min). The research showed that only exercise machine Nr. 3 ensures the possibility to regulate the resistance force proportionally to the resistance level set by control ring on hydraulic cylinder.

Such instability of the force characteristics of rowing exercisers may be caused by design features of the adjusting cylinders.

Resistance force generated by hydraulic cylinders of different rowing machines (at resistance level VIII) was from 50 to 110 N at the lowest velocity of the piston to 150 to 210 N at the highest velocity of the piston, and steppers cylinders gave correspondingly 50–70 N and 270–450 N.

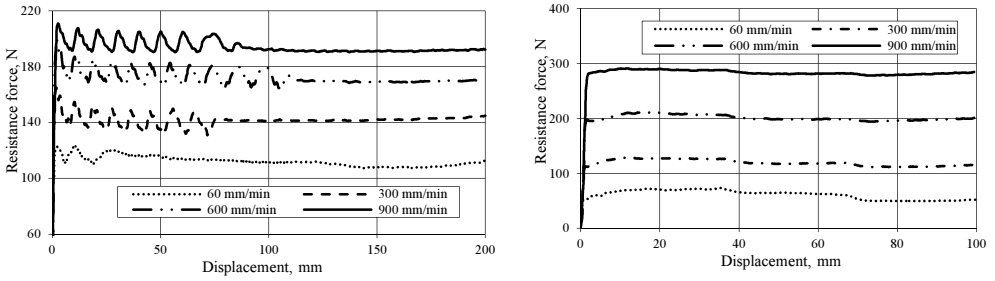

Fig. 1. Resistance force w.r.t. displacement of piston of HC:
a – rowing machine Nr. 1 (resistance level VIII); b – stepper Nr. 5

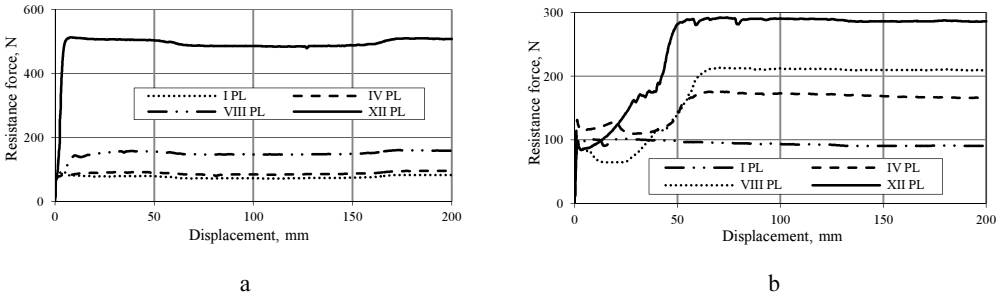

Fig. 2. Resistance force w.r.t. displacement of piston (with 900 mm/min velocity) of HC:
a – rowing machine Nr. 2; b – rowing machine Nr. 3 (at resistance levels I, IV, VIII and XII)

Conclusion

The range and character of variation of the resistance force of hydraulic cylinder type loading units of different exercise machines were obtained. The experimental research showed that resistance force generated by hydraulic cylinders of rowing simulators acting in different regimes differs for each machine and is quite uneven: the variation of resistance force is about 30% of steady force at constant velocity of the piston. Also it was obtained that setting different levels of resistance for rowing machines changes resistance force irregularly.

References

[1] **Grigas V., Legha A., Tolocka R.T.** Simulation possibilities of controlled rowing force generated by hydraulic loading unit of training facility. ISBN 1392 – 1207. Mechanika. 2009. Nr. 2 (76), p. 65–68.

[2] **Zatsiorsky, V. M.** Science and practice of strength training. Human Kinetics, 1995, p. 243, ISBN 0-87322-474-4.

[3] Exercises machines with hydraulic resistance devices. Available from: http://www.fitexpress.com/pages/hydraulic-fitness-equipment.html

[4] Universal exercises machine “HealthMax”. Available from: http://www.healthfxamerica.com/fullvu.htm

Investigation of Functional State of Spine and Paravertebral Tissues and Review of Assessment Methods

A. Juocevičius[1, 2], **S. Lenickienė** [1, 2], **A. Šešok**[3], **E. Jablonskytė**[4], **T. Aukštikalnis**[5], **K. Pakalnienė**[6]

[1]Department of Rehabilitation, Medicine of Physical Culture and Sport, Faculty of Medicine, Vilnius University, Vilnius, Lithuania
[2, 4, 5] The Centre of Rehabilitation, Medicine of Physical Culture and Sport, Vilnius University Hospital „Santariskiu Klinikos“, Vilnius, Lithuania
[3, 6] Vilnius Gediminas Technical University, Lithuania
E-mail: [1]*alvydas.juocevicius@santa.lt,* [2]*svetlana.lenickiene@santa.lt,* [3]*andzela.sesok@vgtu.lt,* [4]*elenytes08@yahoo.com,* [5]*aukstikalnis@gmail.com,* [6]*dargytek@gmail.com*

Keywords: Spine, back pain, functional state, neurospinal functional index.

Introduction

Back pain and related health disorders nowadays are important healthcare problem [1]. Back disease “becomes younger” since more young people suffer from it. Disorders of functional state of spine and balance of strength and stamina of surrounding muscles are one of the causes of back pain related health disorders [1, 2]. Back pain is the most frequent complaint of employable people. Lasting work in awkward position or in badly equipped, nonergonomic workplaces provokes headaches, neck pain, neck and shoulder pain and back pain. Increasing number of research proves relation of back pain and neck pain to smoking, obesity, depression, exercise at leisure time, poor socio-economic status, genetic factors etc. [3].

Functional disorders of spine mostly are reversible, i.e. temporary. Medical rehabilitation is necessary aiming to reduce pain and frequency of illness recurrence, to increase functional ability of the patient and quality of life, to reduce level of disability [4]. Functional disorders of spine often originate from functional block of spinal segments. Functional block may occur both in healthy spine and because of morphological changes (e.g. in osteochondrosis). Functional disorder of spinal motion segment manifests by limited movements [2].

Goniometry [5] is used to assess the functional state of spine though it only enables to measure flexibility of spine and physiological flexures. Complete examination of spinal function is used rather seldom.

The goal of the study was to carry complete examination of different groups of persons (taking exercise and having no back pain, taking exercise and complaining of back pain and patients having back pain and participating at rehabilitation programme) and review diagnostic value of methods used for assessment of functional state of spine and paravertebral tissues.

Methods

45 volunteers (22 females and 23 males) participated in the study. Their age was from 20 to 45 years. The participants were divided into 3 groups. In group 1 were included patients having back pain and performing rehabilitation programme at the Centre of Rehabilitation, Medicine of Physical Culture and Sport of the Vilnius University Hospital „Santariskiu Klinikos“. Persons having back pain and exercising for 3–4 hours per week were included in group 2. The last, control group was composed of persons exercising for 3–4 hours per week and having no complaints. All participating persons were informed about the aims and procedure of the study and signed consent to participate in the study.

Experimental analytical methods were used in the study. “The Insight Subluxation Station” (USA), a computerized equipment, goniometry, visual pain scale (pain index from 1 to 10 points) were used. “The Insight Subluxation Station” (USA) allows to evaluate integrated 5 parameters: 1) state of paravertebral muscles registering electrical activity expressed in microvolts (μV) of muscles by the method of static electromyography using surface electrodes 2) spine flexibility in cervical and lumbar region in sagittal and frontal plane expressed in degrees (°), using wireless inclinometer; 3) influence of autonomic nervous system to functional state of paravertebral tissues by thermoscanner measuring deviations of skin temperature expressed in degrees Celsius (°C); 4) variability of heart beat frequency at rest using pulse wave record contour and 5) pain tolerance limit of paravertebral tissues expressed in kg/cm^2, using algometer. The computerized equipment calculated “neurospinal functional index” (NSFI), an integrated index of all 5 parameters the final result of examination evaluating in points from 0 to 100.

Results

Analysis of electromyographic results of investigated groups showed disbalance of activity of spinal muscles manifested in different groups of muscles: certain groups of muscles were overstretched the overstretching being compensated by other groups of muscles and causing back pain. Inclinometry has shown the greater spine mobility of the group exercising and having no complaints comparing with both the group of persons exercising and having pain and the group of patients. Thermoscanning did not show absolute temperature equality between both sides of spinal muscles, small variation was noted. Greater temperature differences were revealed in the spinal zones with more pronounced muscle overstretching. Pulse variability index has shown absence of balance between sympathetic and parasympathetic nervous system. Even 80% of persons examined had dominant sympathetic nervous system. Such dominance is response to stress, having too much effect in modern world. Exercising persons experiencing back pain better tolerated pain: while pressing mechanically painless area by algometer they felt discomfort at the force of 8.64 kg/cm^2. Discomfort was noted at the force of 5,79 kg/cm^2 while pressing the painful area. Less pressure caused discomfort in patients‘group: force of 7,51 kg/cm^2 for painless area and force of 4,23 kg/cm^2 for painful area.

Conclusions

1. Complex evaluation of functional state of spine in different groups revealed differences in activity of spinal muscles, spine mobility, activeness of sympathetic nervous system, tolerance to pain.

2. The equipment used enabled to find causes of pain that were not discovered by other diagnostic methods, to choose more precisely a complex of rehabilitation means and to assess effectiveness of rehabilitation.

References

[1] **Kopec J. A.** Measuring functional outcomes in persons with back pain: a review of back-specific questionnaires. Spine, 25, 2000, p. 3110–3114.

[2] **Waddell G.** The Back Pain Revolution. Elsevier, 2004.

[3] **Leboeuf–Yde, Charlotte D. C.** Smoking and Low Back Pain: A Systematic Literature Review of 41 Journal Articles Reporting 47 Epidemiologic Studies. Spine, Vol. 24, Issue 14, 1999, p. 1463–1469.

[4] **Lenickienė S., Juocevičius A., Skvereckaitė V.** Effectiveness of the outpatient comprehensive rehabilitation programme. Gerontoligija, XI (4), 2010, p. 211–218

[5] **Tousignant M de Bellefeuille L., O’Donoughue S., Grahovac S**. Criterion Validity of the Cervical Range of Motion (CROM) Goniometer for Cervical Flexion and Extension. Spine, Vol. 25, Issue 3, 2000, p. 324–330.

Load Control by Active Materials at Arm Exercising

V. Eidukynas[1], R. Maskvytis[2], I.Tiknevičienė[3], R. T.Toločka[4]

[1, 2, 3, 4] Kaunas University of Technology, Lithuania
E-mail: [1]*valdas.eidukynas@ktu.lt,* [2]*robertasmaskvytis@yahoo.com,* [3]*irena.tiknevičienė@ktu.lt,* [4]*tadas.tolocka@ktu.lt*

Abstract. Up-to-date training facilities are developed which are able to control loading in order to adapt to the trainee physical abilities, the aim of exercises and make the loading as close as possible to specific sports movements. The arm exercising is simple and effective, thus widely used in practice. Its disadvantage is instability of the arm loading due to inertia forces acting on the lifted mass and changing the arm geometry when exercising. The paper deals with the analysis of possibilities to control the law of loading during the exercising cycle by means of magnetorheological fluid damper.

Keywords: arm exercising, loading, magnetorheological fluid, control.

Introduction

In the present society, sports, active leisure, healthy aging and rehabilitation are in the focus of rapidly growing interest. A wide variety of equipment exists and continues to be developed for such activities. The modern facilities are equipped with feedback between the human input and generated loading, which is used to control the latter in order to achieve the law of its exchange adequate to training aims and workload units, whose action is based on very different principles, are developed to accomplish the task [1, 2].

Active materials have now revealed themselves as extremely perspective for exploiting them in adaptive mechanical devices. A lot of new devices and their composite structures are being created in addition to "classical" ones (rheological fluids, piezomaterials, shape memory alloys). Magnetorheological fluids (MRF) have found application in sports engineering products due to their ability to change rapidly their viscous resistance force using magnetic field as control [3].

The paper discusses the analytical investigation of MRF damper application possibilities to control the load in any training device where muscle loading is created by lifting the mass.

Dynamics of arm loading in the system with MRF damper

Hand motion $y(t)$, when exercising by lifting mass, was measured experimentally, and thus proved it could be quite exactly approximated by fourth degree polynomial. The MRF, approached as Bingham plastic fluid, movement in the damper has been described by equation

$$\rho\frac{\partial^2 u}{\partial t^2}=\eta\frac{\partial^3 u}{\partial x^2\partial t}; \tag{1.1}$$

where ρ is MRF density; η – MRF viscosity; u – MRF fluid particle coordinate,

with initial

$$u\left(x=h,t\right)=s; \qquad \dot{u}\left(x=h,t\right)=\dot{s}, \text{ when } t=0, \tag{1.2}$$

and boundary

$$u\left(x,t\right)=s; \quad \dot{u}\left(x,t\right)=\dot{s}, \text{ when } x=h \text{ and } u\left(x,t\right)=0 \quad \dot{u}\left(x,t\right)=0, \text{ when } x=0, \tag{1.3}$$

conditions, which corresponds to the dynamic model of arm exercising, given in the Fig. 1, in which the elastic and damping properties of rope are evaluated as well.

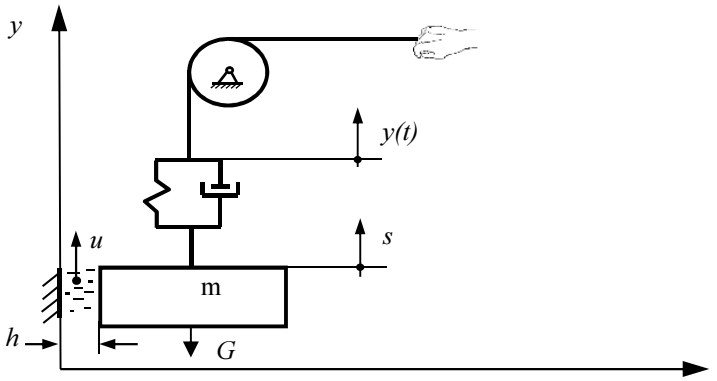

Fig. 1. Dynamic model of arm exercising

The viscous resistance force of MRF has been derived as

$$F_{vr}(\dot{s}) = \sum_{k=1}^{\infty} (\lambda_k \eta ctgh)\dot{s}; \quad \text{where} \quad \lambda_k = \frac{(2k+1)}{2h}\pi, \tag{1.4}$$

which was substituted into the equation describing the given above dynamic model and its solution allowed us to define the law of motion of the lifted mass evaluating MRF damper dynamical properties.

Conclusions

The performed analysis of the training facility with a MRF damper for arm exercising, allowing to evaluate the of MRF viscous resistance influence on the trainee's arm loading, provides a possibility to organize the control satisfying the given requirements on the arm and its muscle loading on the base of the findings.

References

[1] **Zatsiorsky V. M., Kraemer W.J.** Science and practice of strength training. 2nd ed. Human Kinetics. 1995, p. 251–255.

[2] **Shunji M., Sung J.Y., Seok H.K., Motohiro T., Yasuhiko O., Nobuou M., Takakazu I**. A training machine with dynamic load-control function based on muscle activity information. Artif. Life Robotics. Vol. 10, 2006, p. 126–130.

[3] **Carlson J. D., Jolly M. R**. MR fluid, foam and elastomer devices. Mechatronics. Nr. 10, 2000, p. 555

Development of a dynamic model of a cyclist's lumbar spine

Julius Griškevičius[1], **Artūras Linkel**[2]

[1, 2] Vilnius Gediminas Technical University, Lithuania
E-mail: [1]*julius.griskevicius@vgtu.lt,* [2]*linkel.arturas@gmail.com*

Abstract. A dynamic model of a bicyclist's lumbar spine was developed to evaluate the linear and angular variation of intervertebral distance in sagittal plane. Ten degrees of freedom biomechanical model of the spine was solved numerically. Larger loads acting on a cyclist spine were predicted mostly while sitting in a sport position in comparison with recreation or middle sitting. The load on the lumbar spine region is influenced by cycle's tire pressure, road bumps and riding velocity.

Keywords: spine, biomechanical model, dynamics, bicycling, accelerometry, force.

Introduction

Spine diseases and pain are a common social problem in Lithuania and other world countries. Mostly problem occur in the lumbar spine and are summarized as low back pain (LBP) syndrome [1, 2]. LBP and other spinal diseases are a common problem in cyclists, because they have to orient the spine in parallel with the horizontal plane for reaching the best aerodynamic position. Due to back overload about 30% of cyclists after race have to be consulted by a physician. Often the corresponding diagnosis is made as "undefined chronic pain" as a result of lack of spine biomechanics' investigations [3]. Severe back pain most often arises from physical disruption of spinal structures like intervertebral discs, apophyseal joints and sacroiliac joints [4]. Prolonged flexed posture during cycling influences muscle fatigue and increased mechanical strain of the lumbar spine [5, 6]. Also riding surface unevenness can influence overall comfort during bicycle rides [7]. The aim of this study is to develop a dynamic model of cyclist's lumbar region of the spine and evaluate the intervertebral distance variation which depends on wheeling regime and cyclist sitting position.

Materials and methods

Assuming that the main loading of the lumbar spine comes from the contact between bicycle seat and riders buttock during the riding on different surfaces and with different velocity, experimental measurements of the accelerations acting on the cyclist were performed. 2-axial accelerometer ADXL320 was mounted on the seat-post of the bicycle so that sensitive axes were coincident with driving direction and vertical axis. By varying tire pressure and speed while driving on two different road surfaces various spine loading scenarios were evaluated. In order to investigate intervertebral linear and angular displacements a ten degrees of freedom dynamical model consisting of 5 lumbar region spine vertebrae was developed (Fig. 1) and system of 10 second order differential equations of motion (1) (for simplicity only two equations for 1st body are shown) were deduced using Lagrange energy method.

$$\begin{cases} m_1\ddot{x}_1 + \dot{x}_1\left(c_{121}+c_{221}+c_{12}+c_{11}\right) - \dot{x}_2\left(c_{121}+c_{221}\right) - \dot{\varphi}_1\left(c_{121}a+c_{11}a-c_{12}b-c_{221}b\right) - \dot{\varphi}_2\left(c_{221}b-c_{221}a\right) + \\ +x_1\left(k_{121}+k_{11}+k_{221}+k_{12}\right) - x_2\left(k_{121}+k_{221}\right) - \varphi_1\left(k_{121}a+k_{11}a-k_{121}b-k_{12}b\right) + \varphi_2\left(k_{121}a-k_{221}b\right) = F_{t1}+F_{t2}, \\ J_1\ddot{\varphi}_1 - \dot{x}_1\left(c_{121}a+c_{221}b+c_{11}a+c_{12}b\right) + \dot{x}_2\left(c_{121}a-c_{221}b\right) + \dot{\varphi}_1\left(c_{121}a^2+c_{11}a^2+c_{221}b^2+c_{12}b^2\right) - \\ -\dot{\varphi}_2\left(c_{121}a^2+c_{221}b^2\right) - x_1\left(k_{121}a+k_{11}a-k_{221}b-k_{12}b\right) + x_2\left(k_{121}a-k_{221}b\right) + \varphi_1\left(k_{121}a^2+k_{11}a^2+k_{221}b^2+k_{12}b^2\right) - \\ -\varphi_2\left(k_{121}a^2+k_{221}b^2\right) = M_1 - F_{t1}a + F_{t2}b, \end{cases} \quad (1)$$

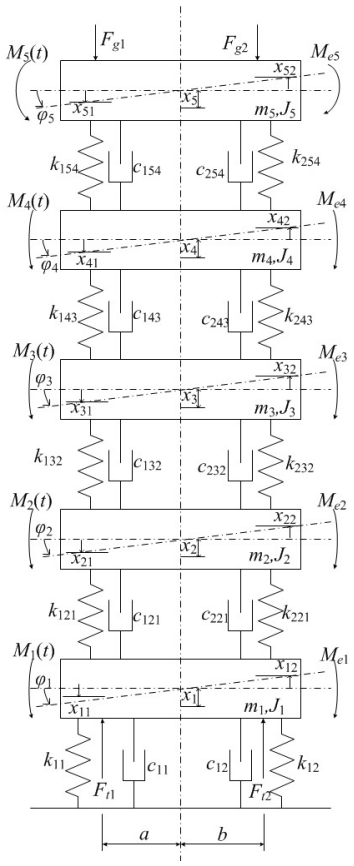

Fig. 1. Dynamic model of cyclist's spine lumbar region: J_i – moments of inertia, x_i – mass displacements, x_{i1}, x_{i2} – mass position variation because of rotation

Intervertebral discs stiffness, damping constants [8] and vertebra's inertial characteristics [9] were chosen from scientific literature. The sitting position of the cyclist affects the load on the lumbar spine. Therefore three spinal inclination angles representing three sitting postures (sport, middle, recreational) were chosen. The external moment M_{ei} due to the sitting position was used to simulate the loading in the biomechanical model.

To solve the equations of motion a variable order method based on numerical differentiation formulas, which is designed specifically to deal with stiff differential systems of equations, was used. This method helped to determine parameters of the lumbar spine, i.e. linear and angular displacements during each wheeling regime and sitting position at cycling. The largest linear and angular displacements were found between vertebrae L4-L5. This can be explained by the increase of a moment arm and concentration of a mass at this place.

Results and Conclusions

At 30 km/h speed and 3.5 bar tire pressure cyclist lumbar spine the model predicted maximum loads of approximately 3.2 kN parallel to the x axis during riding on asphalt and approximately 4 kN on a gravel road. During riding external frequency distributes in rage from 10 Hz to 40 Hz. The largest loads were determined for a sitting position. Maximum vertebrae angular and linear variation values at riding regime with 1.5 bar tires pressure and at 10 km/h speed are 0.46˚ and 0.46 mm. Maximum vertebrae rotation and linear variation values at riding regime with 3.5 bar tires pressure and at 30 km/h speed are 3,9˚ and 1.23 mm. The biggest variation of rotation in sagittal plane between two nearest lumbar spine is about 1˚. Because of this displacement frontal part of last mentioned disc is compressed with 530 N more and dorsal disc part as many less.

References

[1] **Valeikienė V., Mereckas G.** Acute and chronic back pain of older patients. Gerontologija 2006, 7, 3, p. 154–157 (*article in Lithuanian*).

[2] **Hunt T.** Pain in Europe – A report. Cambridge University, 2007, p. 24.

[3] **Salai M.** Effect of changing the saddle angle on the incidence of low back pain in recreational cyclists. British Journal of Sports Medicine, 1999, 33(6), p. 398–400.

[4] **Adams M.A., Dolan P.** Spine biomechanics. Journal of Biomechanics, 2005, 38(10), p. 1972–1983.

[5] **Vey Mestdagh K.** Personal perspective: in search of an optimum cycling posture. Applied Ergonomics Journal, 1998, 5(29), p. 325–334.

[6] **Marsden M.**, **Schwellnus M.** Lower back pain in cyclists: A review of epidemiology, pathomechanics and risk factors. International SportMed Journal, 2010, 11(1), p. 216–225.

[7] **Waechter M., Riess F., Zacharias N.** A multibody model for the simulation of bicycle suspension systems. Vehicle systems dynamics, 2002, 37(1), p. 3–28.

[8] **Kurutz M.** In vivo age- and sex-related creep of human lumbar motion segments and discs in pure centric tension. Journal of Biomechanics, 2006, 39(7), p. 1180–1190.

[9] **Gardner-Morse M., Stokes I.** Structural behaviour of human lumbar spinal motion segments. Journal of Biomechanics, 2004, 37(2), p. 205–212.

Research of Parkinson's disease affected upper extremity biomechanics

Julius Griškevičius[1], **Jurgita Žižienė**[2], **Patrick Mark Aubin**[3]

[1, 2] Vilnius Gediminas Technical University, Lithuania
[3] Wyss Institute for Biologically Inspired Engineering, USA
E-mail: [1]*julius.griskevicius@vgtu.lt,* [2]*biome@vgtu.lt,* [3]*aubin@seas.harvard.edu*

Abstract. In this paper we investigate the biomechanics of upper extremity of Parkinson's disease (PD) subjects in order to create an alternative quantitative diagnostic tool that could be used in clinical setting during diagnosing and monitoring PD. Wireless inertial sensors were used to measure angular velocity and acceleration during multi-joint arm motion tasks from ten PD and ten control (CO) subjects. Mean rest tremor was statistically significantly different between the PD and CO groups. Estimated maximum joint torque values of shoulder and elbow joints were statistically significantly different between the CO and PD groups.

Keywords: Parkinson's disease, biomechanics, upper extremity, wireless inertial sensor, OpenSim.

Introduction

Parkinson's disease is neurodegenerative movement disorder characterized by bradykinesia, rigidity, resting tremor and postural instability [1]. Despite the fact, that PD is a common disorder, accurate diagnosis remains challenging especially in early stages of the disease. Typically, PD is diagnosed clinically using Unified Parkinson's Disease Rating Scale (UPDRS). There are other rating scales, although have not been fully evaluated for validity and reliability [2, 3]. In this study we collected upper extremity kinematic data from PD and healthy control (CO) subjects and investigated features and metrics that may aid in quantitative diagnosis. Our long term goal of this research is to discover biomechanical markers of PD in order to facilitate clinical diagnosis and monitoring of the disease progression.

Methods and materials

Research was carried out on volunteers who were divided into two groups – 10 CO subjects (6 men, 4 women, aged: 65 ± 8 (mean ± SD)) and 10 PD subjects (5 men, 5 women, aged: 71 ± 7 (mean ± SD)). Three wireless sensors, each able to measure linear acceleration, angular velocity and magnetic heading in three dimensions were attached to each patient's hand, forearm and arm (Fig. 1). For the arm and forearm the x–y plane of the sensor's coordinate system was aligned as best as possible to the sagittal plane of the subject. Sensors recorded data at 51.2 Hz. The subjects performed three tremor tasks and eight sagittal plane upper extremity movement tasks. Three tasks each requiring increasing amounts of shoulder joint flexion were performed with and without a dual contralateral open-close hand task.

The tremor tasks consisted of a rest (hand on lap), action (repeated nose touching) and postural (arm outstretched) task. MATLAB software was used to calculate the root mean squared (RMS), peak-to-peak (Pk-Pk), power in 3–8 Hz frequency band (PR) and approximate entropy (ApEn) of the hand's acceleration signal. A one-way ANOVA with a significance level of $\alpha = 0.05$ was used to test the null hypothesis that the RMS, peak-to-peak, 3 to 8 Hz power and approximate entropy in the rest, postural and action tremor signals were the same between the PD and CO groups. The following metrics were calculated from the sagittal plane multi-joint reaching tasks: shoulder and elbow joint peak velocity (PV °/s), reaction time (RT s), dwell time at target (DT s) and maximal joint torque for shoulder and elbow joints (T_s and T_e Nm). The last

parameters (T_s and T_e) were estimated from the inverse dynamics analysis of the recorded motion of the upper extremity using a musculoskeletal model of an arm and OpenSim software.

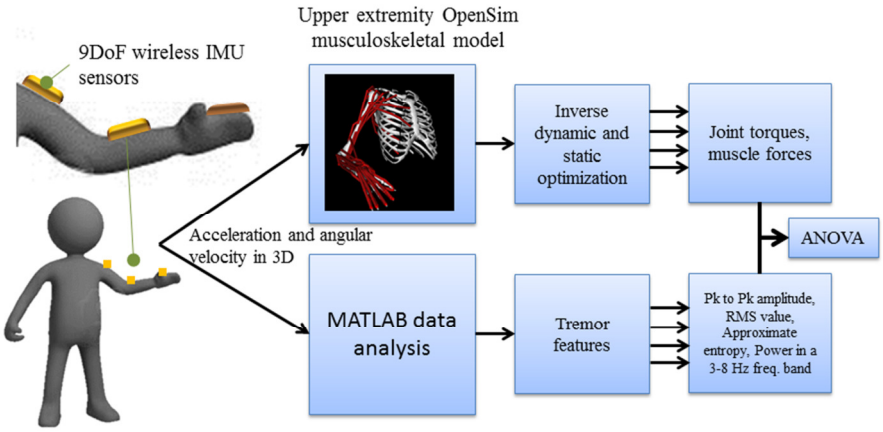

Fig. 1. Upper extremity motor biomechanics evaluation setup

Two-way repeated measures ANOVAs with a significance level of $\alpha = 0.05$ were used to test three null hypotheses: that the means of the metrics (peak velocity, reaction time, dwell time, peak acceleration) grouped by disease type were the same; that the means of the metrics grouped by the dual/non-dual tasks were the same; and that there is no interaction between the disease types and dual/non-dual factors. A one-way ANOVA with a significance level of $\alpha = 0.05$ was used to test the null hypothesis that the maximal joint torques values were the same between the PD and CO groups.

Conclusions

In general we found the feature that best distinguished PD patients from CO subjects was their rest tremor, as measured by either an RMS or Pk-Pk metric. For the rest tremor the mean (SD) of the RMS, Pk-Pk, and ApEn were 0.912 m/s^2 (0.916 m/s^2), 3.128 m/s^2 (3.323 m/s^2), and 0.802 (0.332) respectively for the PD group. These three means were found to be statistically significantly different than the mean RMS, Pk-Pk, and ApEn, for the CO group which were 0.061 m/s^2 (0.008 m/s^2), 0.159 m/s^2 (0.020 m/s^2), and 1.285 (0.040), respectively. For the upper extremity multi-joint movement tasks we found no statistically significant differences between the PD and CO groups regardless of the metric analyzed (PV, RT and DT). It was estimated, that the max shoulder torque (SD) T_s = 43.7 (3.9) Nm and elbow T_e = 16.6 (1.5) Nm for CO group were found to be statistically significantly different (p = 0.03 for shoulder joint and p = 0.02 for elbow joint respectively) for PD group (T_s = 20.8 (2.2) Nm and T_e = 7.6 (0.7) Nm).

References

[1] **Suchowersky O., Reich S., Perlmutter J., Zesiewicz T., Gronseth G., Weiner W.J.** Practice Parameter: Diagnosis and prognosis of new onset Parkinson disease (an evidence-based review): Report of the Quality Standards Subcommittee of the American Academy of Neurology, Neurology, 2006, (66), p. 968–975.

[2] **Ramaker C., Marinus J., Stiggelbout A. M., Johannes Van Hilten B.** Systematic evaluation of rating scales for impairment and disability in Parkinson's disease, Movement Disorders, 2002, (17), p. 867–876.

[3] **Ebersbach G., Baas H., Csoti I., Müngersdorf M., Deuschl G.**, Scales in Parkinson's disease, Journal of Neurology, 2006, (253), Suppl. 4: IV32–35.

Stress analysis in the restored blood vessels by increasing the radius of the transcatheter angioplasty

M. Mariūnas[1], **Z. Kuzborska**[2]

[1, 2]Vilnius Gediminas Technical University, Department of Biomechanics, Vilnius, Lithuania
E-mail: [1]*mecislovas.mariunas@vgtu.lt,* [2]*zyta.kuzborska@vgtu.lt*

Abstract. This paper examines the stress in the restored blood vessels by increasing the radius of the transcatheter angioplasty. The research results show, that expanding blood vessel radius, stresses and displacements increase; it depend on blood vessel medium. More stiff vessels medium characteristics more deformed are plates and blood vessel radius increase.

Keywords: stress, displacement, pathology, transcatheter angioplasty, medium vessels.

Introduction

Many people in the world die from atherosclerosis. It damages vital blood vessels-arteries that carry blood with oxygen and food to the body's tissues. Atherosclerosis plates usually are found in the coronary, carodit arteries and aorta [1, 2, 4, 5].

Damages, caused by atherosclerosis, change blood vessels radius and wall thickness [6]. Depending on damage degree in blood vessel, expanding radius of blood vessels, stresses and displacements could reach dangerous limit. Analysis of scientific works show, that little attention is paid for research of stresses and displacements, performing blood vessels transcatheter angioplasty. Mostly stents are modeled and PTCA (PTCA – Percutaneous Transluminal Coronary Angioplasty) balloon influence to blood vessels is not performed i.e. how distribute stresses and displacements in the pathology area [3, 4].

The aim of this work – to find out stresses and displacements values expanding pathology blood vessels using transcatheter angioplasty (when there is symmetrical and asymmetric radius stenosis), estimating vessels medium and it strength characteristics.

Methods

To determine stresses and displacements in the pathological blood vessels, atherosclerosis with symmetrical and asymmetrical plate was analyzed.

Modeling was performed using ANSYS software package. Linear pathological blood vessel model was made. By evaluating the condition of deformed blood vessel and chosen finite element the 3% validation of calculation results was performed. Research was performed using two dimensional and three dimensional arterial blood vessel models.

Results

The research results show, that expanding blood vessel in damaged areas using transcatheter angioplasty, stresses in blood vessels are very high (Fig. 1 and 3), if will be no blood vessel medium, it could crack. Blood vessel displacements – Δu, when pressure $p = 2.35$ MPa, reach critical crack limit (Fig. 2 and 4) and stresses also reach blood vessel crack limit.

Performed analysis show, that expanding blood vessel using transcatheter angioplasty, its radius increase from 25 to 58% when vessel medium is plate-vessel. In medium plate-vessel-adipose tissue-muscle, blood vessel radius increase from 25 to 66%.

That way, when there is different blood vessel medium, blood vessel radius could be increased with lower pressure balloon and to decrease stresses in the blood vessel.

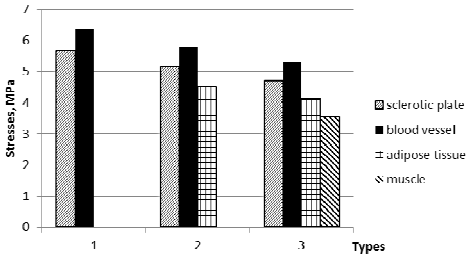

Fig. 1. Stress distribution of coronary artery

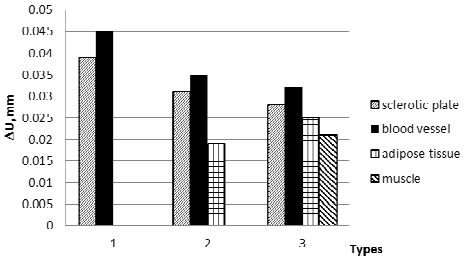

Fig. 2. Displacement distribution of coronary artery

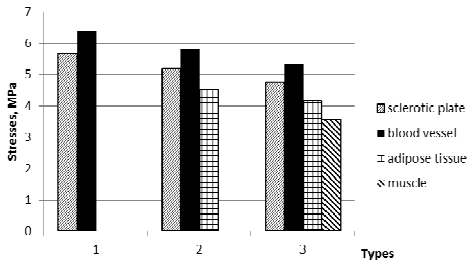

Fig. 3. Stress distribution of carotid artery

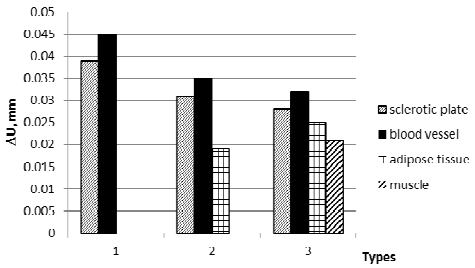

Fig. 4. Displacement distribution of carotid artery

In asymmetric case, expanding blood vessel, different mediums and different characteristics influents features occur. In the blood vessel side with sclerotic plate, stresses could reach critical limit and in opposite side lump could occur. Where blood vessel medium is minimal, stresses and displacements are big and dangerous.

Conclusions

Expanding blood vessel radius from 25 to 66%, stresses from 1,8 to 6,35 MPa and displacements from 0 to 0.045 mm increase; it depend on blood vessel medium. Medium determine if blood vessel crack or not. More stiff vessels medium characteristics more deformed are plates and blood vessel radius increase. It could be increased to 20%.

In asymmetric case, expanding blood vessel, different medium and different characteristics influents features occur.

References

Bukac M., Canic S. Longitudinal displacement in viscoelastic arteries: a novel fluid-structure interaction computational model, and experimental validation, Mathematical biosciences and engineering, Vol. 10, number 2, April 2013, p. 295–318.

[1] Gu L., Zhao S., Muttyam A.K., Hammel M.J. The relations between the arterial stress and restenosis rate after coronary stending, Journal of Medical Devices, Vol. 4, 2010, p. 031005–7.

[2] Huang J., Lyczkowski R.W., Gidaspow D. Pulsatile flow in a coronary artery using multiphase kinetic theory, Juornal Biomechanics, Vol. 42(6), Apr 2009, p. 743–54.

[3] Liang D., Yang D., Qi M., Wang W. Finite Element Analysis of a Stent Implantationin a Stenosed Artery. Key Engineering Materials, Vol. 288–289, 2005, p. 571–574.

[4] Lindsay C. H. John. Biomechanics of Coronary Artery and Bypass Graft Disease: Potential New Approaches, The Annals of Thoracic surgery, Vol. 87, 2009, p. 331–338.

[5] Mariūnas M., Kuzborska Z. Influence of load magnitude and duration on the relationship between human arterial blood pressure and flow rate. Acta of Bioengineering and Biomechanics, Vol. 13(20), 2010, p. 67–72.

Modelling and research of durability of the Ankle-Foot Orthosis

Andžela Šešok[1], **Oleg Ardatov**[2]

[1, 2] Vilnius Gediminas Technical University, Department of Biomechanics, Vilnius, Lithuania
E-mail: [1]*andzela.sesok@vgtu.lt,* [2] *oleard@gmail.com*

Keywords: Ankle biomechanics, Ankle-Foot Orthosis (AFO), Research of durability, Finite Element Analysis.

Introduction

Pathological motion of the ankle-foot complex presents a major problem in the rehabilitation of stroke and head injury patients. For example, stroke patients often develop "drop foot", a problem involving excessive and uncontrolled plantar flexion. Ankle-foot orthoses (AFOs) are prescribed and used to restore normal motion or to constrain and inhibit abnormal motion. Research projects need to be conducted that include new methods of studies and experimental testing in which a better design could be achieved and appropriate prescription could be applied [1]. Historically, orthotic devices have been used for the treatment of musculoskeletal injuries or dysfunctions and have provided support, protection, immobilization, and correction [1]. The most popular materials for orthoses are polypropylene (PP) and polyethylene (PE) due to their high fatigue resistance, high strength, light weight, and excellent molding characteristics. PP is heat sensitive and can be molded into every thin-walled orthosis when it is warm; more grinding, fixing, and modifications are needed after the device becomes cold [1, 2]. Taking into account that the process of treatment of arthronosos is usually long-lasting and often the patient is forced to use an orthosis for all his/her life, durability of the orthosis is of a particular importance. The issue of foot orthoses' durability has not been thoroughly discussed upon in scientific and technical literature as well as medical publications, and an orthosis for a patient was usually chosen upon taking into account the mechanical properties of its material [2, 3] and ignoring the difference between durability of the orthosis and durability of its material.

The aim of the work is research of durability of Ankle-Foot Orthosis AFO upon taking into account the properties of its material and development of methods for detailed assessing a fitness of an orthosis upon taking into account its durability and other properties in any specific case.

Methods

The simplified structure of the system under discussion, its kinematics and distribution of static forces are presented in Fig. 1. The Fig. 1 shows static loads that affect a standing human (in the sagittal plane). Here q_1 – the distributed load, caused by the contact of the shin with the orthosis. The load q_2 appears because of pressure of the foot onto the surface of the orthosis. It should be noted that while the human is standing of the both feet, the load is equal to a half of his/her weight. In respect of durability, the most dangerous load is the bending moment *M* that appears when the body gravity line is some centimeters in front of the transverse axis of the ankle joint.

On the base of anthropometric norms and the principles of somatography, a three-dimensional model of Ankle-Foot Orthosis was developed in digital *SolidWorks* environment.

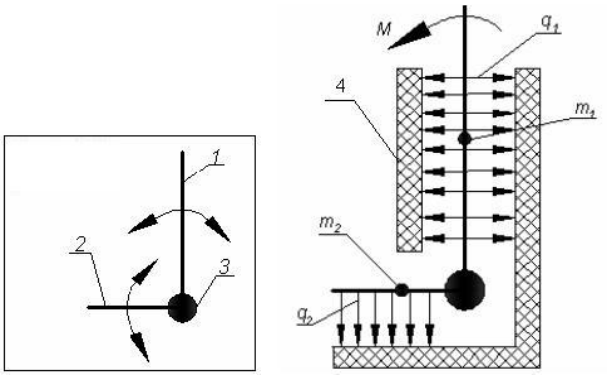

Fig. 1. The model of the ankle joint: 1 – the shin; 2 – the foot; 3 – the joint; 4 – the orthosis

The orthosis is loaded with forces equal to 70, 850 and 1000 N; the chosen thickness of the orthosis is 3, 4 and 5 mm, respectively; the materials of the orthosis are polyethylene (PE) and polypropylene (PP). The mechanical and material properties for the soft tissue, the PP and PE AFO were all assumed to be linear, elastic, and isotropic.

Results

In solution of contact-related tasks, the maximum stresses and shifts of AFO model take place upon the effect of the horizontal component of body gravity force. It was found that abrupt transitions are absent in points of maximum concentration of stresses, so supplemental stress concentrators that may turn into foci of micro cracks do not appear. However, because of the contact between AFO and the foot, a complicated deformation of the orthosis as well as additional compression and stretching of the material take place in adjacent zones and may cause a negative impact upon the durability of the orthosis. In addition, it should be noted that distribution of stresses is asymmetric because of a complicated shape of the orthosis. The typical breaking points of the orthosis models and the numbers of cycles corresponding to them were established. The models produced from high density polyethylene were rather endurant ($3 \cdot 10^7$ cycles of load) compared to those made of polypropylene ($1{,}6 \cdot 10^7$ cycles of load). Thus, the use of polyethylene splints should be extended at bigger loads.

Conclusions

The developed 3D computer model of Ankle-Foot Arthosis enables to forecast the operational life of the Ankle-Foot Orthosis and to choose an orthosis properly upon taking into account the patient's weight, height and degree of mobility as well as the durability of the material of the orthosis. In respect of durability, polyethylene is considerably superior to polypropylene. So, polyethylene is a desirable structural material for foot orthoses. Polypropylene may be used in certain cases for orthoses where the thickness of the material is no less than 5 mm that are usable for patients with a lower degree of mobility.

References

[1] **Tina Taiming Chu.** Biomechanics of Ankle-Foot Orthoses: Past, Present, and Future. Top Stroke Rehabil. 7(4), 2001, p. 19–28.

[2] **Brodsky J.W, Pollo F. E, Cheleuitte D, Baum B. S.** Physical properties, durability, and energy-dissipation function of dual-density orthotic materials used in insoles for diabetic patients Foot Ankle Int. 28(8), 2007, p. 880–900.

[3] **Shaofu W. *et al.*** Defect Analysis and High Density Polyethylene Pipe Durability. Plastics Failure Analysis and Prevention. 21, 2001, p. 281–287.

Research of muscle adaptive biotronic system frequency and amplitude relation

Mečislovas Mariūnas[1], **Kristina Daunoravičienė**[2]

[1, 2] Vilnius Gediminas Technical University, Lithuania
E-mail: [1]*mariūnas@vgtu.lt,* [2]*kristina.daunoraviciene@vgtu.lt*

Keywords: adaptive biotronic system (BS), excitation frequency, amplitude, loading duration.

Introduction

Scientific works [2–9] have shown that in longer muscle loading duration and at higher load, amplitudes of most biosignals are increasing and similarly the value of summary biosignal amplitude is growing [10]. However in the sources [8, 11–13] decrease of muscle biosignal frequency at longer or steady loading was found. Analyzing muscle as adaptive BS was studied the assumption that it works at resonance frequency [1] and this assumption was proved practically, i.e. has been shown that with minimal impact of external energy adaptive system output generate higher amount of energy. However, there were the scientific works those didn't analyze the relation between muscle BS excitation frequency and the oscillation amplitude of biosignal size. Therefore, the aim of this work is to determine the relationship between muscle adaptive BS excitation frequency of the vibration amplitude level, muscle size and distance traveled, or load-term relationship, and experimentally confirm the existence of resonant work conditions.

Methods

Analyzing specific examples the relation between adaptive BS excitation frequency ω_{imp} and amplitude size A_{imp} as well as distance of lifting load h was estimated. Observing the rise in the weight of the athlete was noticed that to the lifted weight was given sudden impulse at the moment of its uplift of the base point. However, if the weight is raised above his head violently – fatigue would be significantly lower. Thus, the assessment of performed work size in one or another case, the inequality can be written: $D_{slow} > D_{imp}$, where D_{slow} is the slow work, D_{imp} is the impulsive work. In the way of impulsive work D_{imp} and by underestimating energy dissipation the equality exists:

$$D_{imp} = Q \cdot h = \frac{mv_{imp}^2}{2} - \frac{mv_0^2}{2}, \quad (1)$$

where Q is the loading weight kg, h stands for lifting height, m is the mass of lifting load, v_{imp} is the velocity of lifting impulse and v_0 stands for initial velocity (at estimating case it would be equal to zero).

After transforming the equality (1) the expression of muscle generated impulse angular velocity has been given: $\omega_{imp} : \omega_{imp} = \sqrt[3]{g \frac{v_h}{A_{imp}}}$, where v_h is average velocity of lifting load Q, A_{imp} is the size of impulse amplitude generated by muscle. As evaluating energy dissipation in the system inequalities (2) should exist. Values of parameters such as loading size F, height h and mass m for appropriate person are constant and only A_{imp} are varying. Therefore, by

decreasing muscle generated impulse angular velocity and for satisfy the condition of resonance work in the system,

$$v_h > \frac{1}{g}\omega_{imp}^3 A_{imp}^2, \quad \omega_{imp} \geq \sqrt{\frac{2Fh}{m}} = \sqrt{2gh} = const, \tag{2}$$

oscillation amplitudes should nonlinearly increase. Furthermore, for every F, m h value is necessary different muscle BS generated impulse frequency and the excitation amplitude. It is seen from the expressions (2) that the value of initial impulse frequency ω_{imp} provided to a load nonlinearly depend on a height and free-fall acceleration g, but is independent of the mass and the weight of athletes. Thus, biosignal excitation frequency must also be varied by the same law, that the condition $E_{imp} > E_{in}$ is met. When a person performs a work carrying the load, the variable "h" in the previous equation by changing the variable "s" or its derivative, we can assess the adaptive BS settings.

Experimental research

By the harmonic analysis made on biosignals of the thumbs short abductor muscle (*m. abductor pollicis brevis*), then the spectrum changes in loading duration and as F = 18 N was noticed that values of spectral low frequencies are diminishing at longer loading duration.

Analyzing changes of the frequency range from 520 to 175 Hz in the loading duration according its upper surrounding line, the reflection at the 7th loading minute is clearly seen. After this time the generation and stimulation frequencies are decreasing. Such situation when biosignal amplitude is increasing at frequency fall is showing approximate resonance conditions in adaptive BS.

Conclusions

After observing analytical and experimental research results there were formulated the following conclusions:

1. Optimal initial impulse values of adaptive BS are estimated in the moment when the weight is raising and the relation with the loading size and a lifting distance is explained.
2. The frequency of the initial impulse and the angular velocity nonlinearly depend on the load lifting distance and free-fall acceleration, but are independent of the person's weight. These parameters should be clearly specified.
3. Experimental research has shown decreasing frequencies in longer loading and their amplitudes vary nonlinearly. The multiplication of these parameter's sizes is approximately constant.
4. Resonance work conditions of adaptive muscle BS were determined.

References

[1] **Mariūnas M.** Research of adaptability of muscle's biotronic system**.** Journal of Vibroengineering, Vol. 10, Issue 2, 2008, p. 257–260.

[2] **Marateb HR, Rojas M, Mansourian M, Merletti M, Mañanas MA (2012)** Outlier Detection in High-Density Surface Electromyographic Signals. Medical & Biological Engineering & Computing, Volume 50, Issue 1, January 2012, p. 79–89.

[3] **Sundstrup E, Jakobsen MD, Andersen CH, Zebis MK, Mortensen OS, Andersen LL**. Muscle activation strategies during strength training with heavy loading vs. repetitions to failure. Journal of Strength Conditioning Research. 2012 Jul; 26(7), p. 1897–903.

Research of stresses distribution in endoprosthesis contact considering the law of stochastic distribution of micro-roughness

Mečislovas Mariūnas[1], **Julius Griškevičius**[2], **Andžela Šešok**[3]

[1, 2, 3] Vilnius Gediminas Technical University, Department of Biomechanics, Vilnius, Lithuania
E-mail: [1]*mariunas@vgtu.lt,* [2]*julius.griskevicius@vgtu.lt,* [3]*andzela.sesok@vgtu.lt*

Keywords: stresses, stochastic distribution of micro-roughness, detrition, deformations.

Introduction

Reliability and durability of endoprostheses work depend on the wear speed of its contact surfaces and on the material properties of the ball and the acetabular [1]. The speed of the wear mainly depends on pressure value in the contact surfaces and the value of the friction coefficient. The wear were analysed in some scientific papers [2–4]. However in those scientific papers pressure or stress distribution in the endoprostheses contact surfaces depending on the gap size between the acetabular and the ball is not clearly investigate. There is a lack of scientific works devoted for the development of stochastic mathematical models [2], and presented models are highly complex. While analyzing contact stiffness and stress magnitude in the contact, most of the authors are stating that contact surface is equal to surrounding surface. Latter assumption does not reflect the reality. In fact the surrounding surface is larger than surrounded. Therefore, actual contact stiffness and stress magnitude in contact can differ from the calculated considering that the contacting surface matches surrounding surface.

The main goal of this research is to develop stochastic mathematical model that would enable to simply analyze the estimation regularities of random values distribution density of two contacting surfaces and to determine distribution of stresses while considering the influence of surface micro- roughness and detrition degree.

Methods and mathematical modelling

In order to calculate of force F_i (1) is necessary to determine of summary distribution density of contacting surfaces micro-roughness random values (2).

$$F_i = c_0 Q_i \left[\delta_i \int_0^{\delta_i} f\left(\Delta_s\right) d\Delta_s - \int_0^{\delta_i} \Delta_s f\left(\Delta_s\right) d\Delta_s \right], \tag{1}$$

where $\Delta_S = \Delta_{R_{ri}} + \Delta_{R_{gi}}$; $f\left(\Delta_s\right)$ – summary distribution density of contacting surfaces micro-roughness random values; δ_i – magnitude of deformation; c_0 – coefficient of proportionality that evaluates strength properties of endoprosthesis material.

$$f\left(\Delta_{R_r}\right) = \frac{1}{\Delta_{R_{ri}}} \quad \text{and} \quad f\left(\Delta_{R_g}\right) = \frac{1}{\Delta_{R_{gi}}}, \tag{2}$$

where $\Delta_{R_{ri}}$ and $\Delta_{R_{gi}}$ – values of micro-roughness of surrounding and surrounded surfaces, when $0 \lhd \Delta_{R_{ri}} \lhd\lhd \infty$ and $0 \lhd \Delta_{R_{gi}} \lhd\lhd \infty$. Applying composition method of distributions of independent random values, i.e. $\Delta_S = \Delta_{R_{ri}} + \Delta_{R_{gi}}$, we can write:

$$f(\Delta_s) = \frac{\partial\left[F(\Delta_s)\right]}{\partial\Delta_s}, \quad f(\Delta_s) = \iint f\left(\Delta_{R_r}\right) f\left(\Delta_{R_g}\right) d\Delta_{R_r} d\Delta_{R_g}, \quad \Delta_{R_{ri}} + \Delta_{R_{gi}} \lhd \Delta_s. \qquad (3)$$

Results

Knowing, that $\sigma_{ij} = \frac{F_i}{Q}$ from (1) we get the expression:

$$\sigma_{ij} = c_0 \left[\delta_{ij} \int_{\delta_{ij1}}^{\delta_{ijz}} \frac{\Delta_s}{\Delta_{R_{r0}} \Delta_{R_{g0}}} d\Delta_s - \int_{\delta_{ij1}}^{\delta_{ijz}} \frac{\Delta_s^2}{\Delta_{R_{r0}} \Delta_{R_{g0}}} d\Delta_s \right], \qquad (4)$$

where i^{th} approach of contacting surfaces, j_k, j_{k+p} – separated interval of p points $0 \le \delta_{ij} \le \Delta_s$ in deformation interval. Integral (4) can be replaced approximately with finite sum.

The variation of calculated deformation values in contact is shown in Fig. 1. Regularity of distribution of stresses in different points of contacting surfaces is shown in Fig. 2. From the Fig. 2 it can be seen that during the wear of endoprosthesis, i.e. the gap between surrounding and surrounded surfaces is increasing, maximal values of stresses increases considerably.

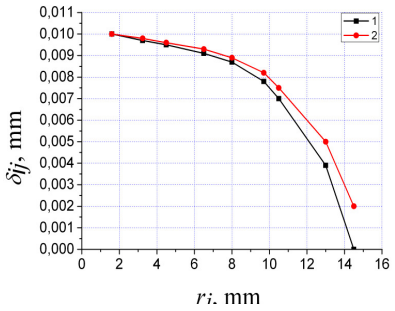

Fig. 1. Dependency of deformation values on the size of surrounding radius: 1 – the gap size between the acetabulum and the ball $\Delta = 0.01$ mm; 2 – $\Delta = 0.005$ mm

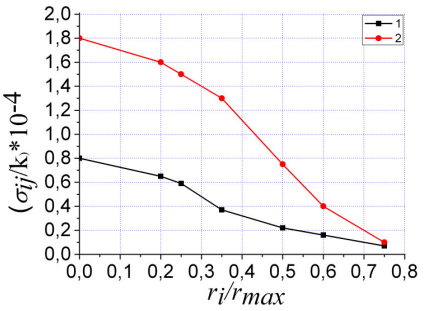

Fig. 2. Distribution of stress ratio in the contact surface of the endoprostheses when: 1 – the radius of the ball R_r =15 mm, Δ = 0,005 mm, δ_i = 0,001mm; 2 – R_r =15 mm, Δ =0,01 mm, δ_i = 0,001 mm

Conclusions

1. The worked out statistical mathematical model allows analyzing the regularities of estimation the law of density distribution of contacting surfaces random values. Evaluating summary micro- roughness distribution of two contacting surfaces estimated stress distribution depending on the wear, deformations and geometrical parameters.

2. The highest stress values are in the center of the contact surface of the endoprostheses. Their values are significantly higher than compared to those in the contact borders.
3. Stresses of the contacting surfaces increases with the increasing degree of surface wear and the maximal values can exceed several times the values for new endoprosthesis.

References

[1] **Mariūnas M., Karavackaitė J.** The Influence of Pressure Distribution in Contact Area upon the Gap Between the Acetabular an the Ball. Mechanika. 2003, Nr. 1(39), p. 52–55.

[2] **Wierzcholski K.** Stochastic impulsive pressure calculations for time dependent human hip joint lubrication. Acta of Bioengineering and Biomechanics. Vol. 14, N. 4, 2012, p. 81–100.

[3] **Wierzcholski K, Nowakowska K.** Pseudo-Gaussian density function for gap height between two surfaces. XIII Journal of Applied Computer Science, 2010, Vol. 18, No. 2, p. 79–90.

[4] **Colombi P.** Fatigue analysis of cemented hip prosthesis: damage accumulation scenario and sensitivity analysis. International Journal of Fatigue. Vol. 24, 7, 2002, p. 739–746.

Reliability analysis: force displacement curve at different loading rate of the amputated foot

Danguolė Satkunskienė[1, 4], **Raminta Sakalauskaitė**[1], **Aurelijus Domeika**[2], **Egidijus Kontautas**[3], **Kristina Kazlauskienė**[4]

[1]Laboratory of Kinesiology, Lithuanian Sports University, Kaunas, Lithuania
[2, 4]Kaunas University of Technology, Lithuania
[3]Lithuanian University of Health Sciences
[1,4]Corresponding authors
E-mail: [1, 4]*danguole.satkunskiene@lsu.lt,* [1]*raminta.sakalauskaite@lsu.lt,* [2]*aurelijus.domeika@ktu.lt,* [3]*egidijuskon@yahoo.com,* [4]*kristina.kazlauskiene@ktu.lt*

Abstract. The aim of our study was to assess the measurement reproducibility of the amputated defrosted foot compression test data at different loading rate. The foot specimen used for testing was from a female. Compressive tests were done on a 25 kN force Tinius Olsen H25K-T testing machine. Defrosted foot specimen was repeatedly loaded at a different rate 25 mm/min, 50 mm/min, 100 mm/min and 500 mm/min. The Intraclass Correlation Coefficient was calculated to assess the measurement reliability of foot force-displacement curves at each loading rate. The measures of foot displacement taken from the repeated compression test had a very high level of agreement at each compression rate.

Keywords: measurement reproducibility, force-displacement curve, foot, compression test.

Introduction

Development of a realistic physics-based human foot model requires the use of empirical data on the mechanical behavior of the foot arch, foot bones, cartilages, plantar ligaments and fascia and heel pads under the action of external forces. To investigate the mechanical properties of foot many authors use the cadaver feet [1–5]. During testing the specimens are loaded repeatedly and it is not clear yet how force displacement curve at different loading rate of the amputated defrosted unfixed foot changes with the increasing number of repetitions. The goal of our study was to assess the measurement reproducibility of the amputated defrosted foot compression test data at different loading rates.

Methods

The specimen was a right foot with normal longitudinal arch from a female. The right limb was amputated due to irreparable vascular disease. At the time of surgical procedure the age of the donor was 64 years; body weight and height were 69 kg and 1.68 m respectively. The foot was disarticulated at the ankle with preservation of all soft tissues. The specimen was evaluated for clinical and radiographic normality by orthopedic surgeons prior to testing. The foot was sealed in double plastic bags and stored in a freezer maintained at –20 °C. It was thawed at room temperature for 24 hours before testing. The National Bioethics Committee reviewed and approved the study protocol.

Compressive tests were done on a 25 kN force Tinius Olsen H25K-T testing machine. The foot was put on the machine so that talus would be in the pressing center. Before the formal trial, the specimen was three times preconditioned to 1000N. Defrosted foot specimen was repeatedly loaded at a different rates 25 mm/min (ten times), 50 mm/min (ten times), 100 mm/min (ten times) and 500 mm/min (four times). The maximum loading 1000N was achieved. There was an interval of 2 minutes between each compression. Before the next loading the foot was put on the machine in new stable position. During compressions the Tinius Olsen H25K-T testing machine indicated the values of displacement (mm) and force (N).

The Intraclass Correlation Coefficient (ICC) was calculated to assess the measurement reliability of foot force-displacement curves at each loading rate.

Results

The measured force-displacement curves taken from the repeated compression tests had a very high level of agreement (Fig. 1). The high values of the Intraclass Correlation Coefficients (25 mm/min ICC = 0.995, p<0.000; 50 mm/min ICC = 0.998, p<0.000; 100 mm/min ICC = 0.999, p<0.000; 500 mm/min ICC = 0.996, p<0.000) showed that the force displacement curves within each loading rate were almost exactly the same.

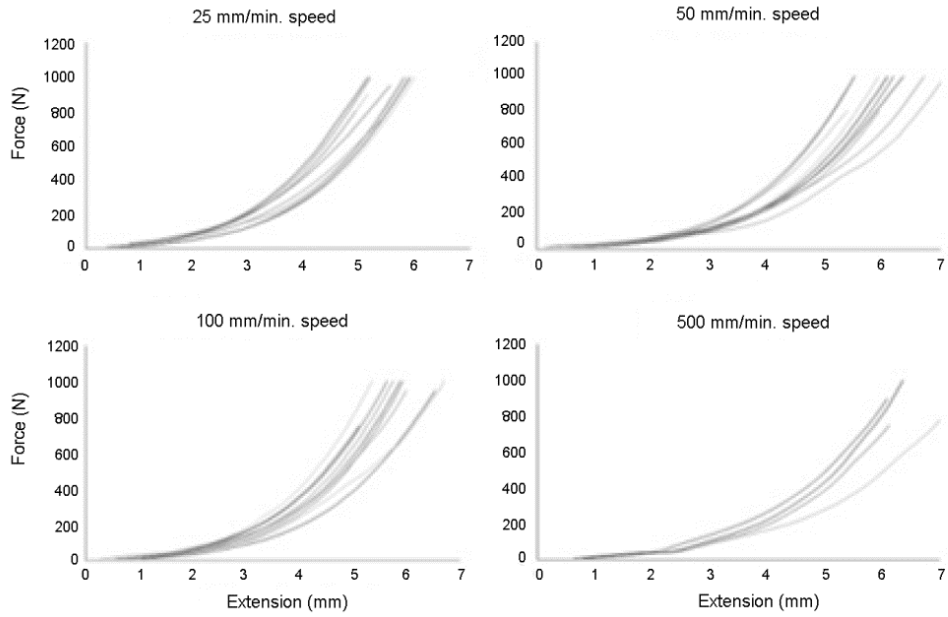

Fig. 1. Force displacement curves at different loading rate of the foot specimen

Discussion

The measurement reliability plays a very important role when the measurement is repeated for the same cadaveric specimen (in an artificial experimental situation). The studies showed that testing feet at room temperature after frozen storage gives the same results as testing fresh and warm feet [6]. The question if the number of loading repetitions has influence on the findings could not be answered. Our data gave a possibility to calculate Intraclass Correlation Coefficients and to assess the measurement reliability of the force-displacement curves of the foot at different loading rates. The findings showed that the number of loading repetitions of the amputated defrosted feet doesn't have influence on compression test data.

Conclusions

We conclude that cadaveric defrosted foot repeatedly loaded during compression test demonstrated very good force displacement curve reliability. This finding was showed at different loading rates.

References

[1] **Erdemir A., Hamel A.J., Fauth A.R., Piazza S.J., Sharkey N.A.** Dynamic loading of the plantar aponeurosis in walking. The journal of bone and jodint surgery, 86 (3), 2004, p. 546–552.

[2] **Suckel A., Muller O., Herberts T., Wulker N.** Changes in Chopart joint load following tibiotalar arthrodesis: in vitro analysis of 8 cadaver specimen in a dynamic model. BMC Musculoskeletal Disorders 8: 80, 2007.

[3] **Niu W., Yang Y., Fan Y., Ding Z., Yu G.** Experimental modeling and biomechanical measurement of flatfoot deformity. IFMBE Proceedings 19, 2008, p. 133–138.

[4] **Erdemir A., Sirimamilla P. A., Halloran J. P., Bogert A. J.** An Elaborate Data Set Characterizing the Mechanical Response of the Foot. Journal of Biomechanical Engineering 131(9), 2009.

[5] **Liang J., Yang Y. F., Yu G. R.** Deformation and stress distribution of the human foot after plantar ligaments release: A cadaveric study and finite element analysis. Sci China Life Sci 54, 2011, p. 267–271.

[6] **Bennett M. B., Ker R. F.** The mechanical properties of the human subcalcaneal fat pad in compression. Journal Anatomy 171, 1990, p. 131–138.

Modified kNN algorithm for automated walking patterns recognition using GRF data

M. Derlatka

Bialystok University of Technology, Poland
***E-mail**: m.derlatka@pb.edu.pl*

Keywords: human gait recognition, k-nearest neighbors.

Introduction

The human gait is the result of synergistic activity of: bones, muscles and nervous systems. The cooperation of those three systems makes the human movement unique for every person. This allows to use human gait as a tool for person recognition [1]. In this case any type of classifier must be used to assign a proceeded walking pattern to one of the subjects stored in database. One of the most frequently used classifier is k-nearest neighbors (kNN). It makes classification based on defined distance from so called prototype points (training set). Unfortunately, kNN algorithm attributes a given point of the space of features to one of the classes even when the distance, though minimal, is as long as we should talk about the lack of similarity to all patterns. In this situation, which is quite often present in biometrics, the desired answer of the classifier is the information of unrecognizing the given person. The main aim of this paper is presenting a modification of kNN algorithm which works properly in biometrics. Test of the presented methods are made on own investigation of human gait

Materials and Method

The measurements were made in the Bialystok University of Technology on a group of 71 students (38 men and 33 women) by means of the two Kistler force plates. The subjects who took part in the investigations were at age 21.18 ± 1.28, BW: 75.68 ± 18.07 kg and BH 174.49 ± 9.54 cm. During investigation almost 1300 gait cycles have been recorded. 355 strides from 71 users were stored in the database and used as so called prototype points. The rest of strides 930 gait cycles were used for testing. The distance between prototype points and all biometrics patterns has been calculated by means of dynamic time warping (DTW) [2].

The DTW calculates the minimal cost of the transformation one time course into other. This investigation take into consideration all ($L = 6$) component of ground reaction forces so the total distance was calculated as:

$$\rho = \sum_{l=1}^{L} DTW_l \tag{1}$$

The 5-nearest neighbors classifier based on the calculated distance has been used to make human gait recognition (Fig. 1). The new version of k-NN is proposed to adjust the typical version for biometric needs. In this work the classification is made with taking into account the similarity level (threshold) between a prototype and proceeding pattern. The user's distance limit depending on the threshold is calculated as:

$$\rho_{\vartheta i} = (1.5 - \vartheta) \cdot \rho_i \tag{2}$$

where: ρ_i – is the average distance between the prototypes points for the i-th user; ϑ – chosen security (similarity) level; $\vartheta = \{0.1; 0.2; \ldots, 0.9\}$.

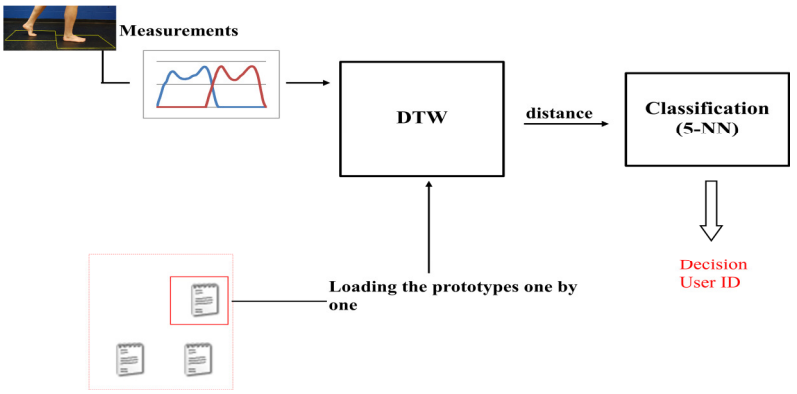

Fig. 1. The scheme of the human gait recognition by means of the typical 5NN classifier

The modified algorithms of k-NN have the following form:

1. Calculate the distance ρ of the proceeding biometrics pattern to all prototypes from the database.
2. Choose the k prototypes which are the nearest neighbors of the proceeding pattern.
3. Use vote method to establish user's ID. If two or more users have the same numbers of prototypes chosen in p. 2 – choose ID of a user who has the smallest average distance.
4. To prune k' prototypes which the distance ρ is longer than user's $\rho_{\vartheta i}$ for the chosen security level ϑ.
5. According to procedure described in p. 3 check if user's ID for K = k-k' prototypes is unchanged. If the user's ID is unchanged the proceeding biometrics pattern has been classified to ID class, otherwise go to p.3.
6. If k=k' there is no possibility to classified the proceeding biometrics pattern to any of existed class with chosen threshold ϑ.

Results

The errors FAR was equal 5.16% and FRR – 3.22% for typical 5-NN.

Table 1. Results of the identification of the users by means of modified 5-NN

threshold	0.1	0.2	0.3	0.4	0.5	0.6	0.7	0.8	0.9
FRR	3.01	3.44	3.76	4.73	6.13	7.53	11.18	16.02	22.8
FAR	2.47	2.37	1.72	1.4	1.29	1.29	1.08	0.43	0.43

The general recognition accuracy is really high especially comparing to works where GRF profiles have been used [1], [3].The results obtained by modified 5-NN is much better than by typical 5-NN classifier in both types of errors for threshold 0.1. The changes of threshold allow fitting the biometrics system to the one's requirements (more flexible or more secure).

Conclusions

The obtained results show that the human gait is a biometric measure which enables efficient authorization. The new version of k-NN adjusts the typical version for biometric needs. It allows for a correct classification of also those cases which have no chances with the classical version of kNN. The whole encourages to continue works in this direction, which, for example more rigorous criteria of threshold ϑ selection, should make a good method of classification still better.

References

[1] **Derlatka M.,** Human Gait Recognition Based on Signals from Two Force Plates. ICAISC'2012 LNCS Vol. 7268: LNAI, 2012, p. 251–258.

[2] **Porwik P.** ***et al***. Biometric Recognition System Based on the Motion of the Human Body Gravity Centre Analysis. Journal of Medical Informatics and Technologies, 2010, 15, 61–69.

[3] **Yao Z.** ***et al*.** A Novel Biometric Recognition System Based on Ground Reaction Force Measurements of Continuous Gait. Human System Interactions. 3rd Conf. on Digital Object Identifier, 2010, Rzeszow Poland, 452–458.

Experimental verification of the uroflowmetry system based on a weight transducer

Wojciech Walendziuk[1], **Adam Idzkowski**[2]

[1, 2]Bialystok University of Technology, Wiejska 45D str., Bialystok, Poland
E-mail: [1]*w.walendziuk@pb.edu.pl*, [2]*a.idzkowski@pb.edu.pl*

Abstract. The aim of this work is the evaluation of metrological properties of the constructed uroflowmeter device. The examination was done on standard flow samples, dosed by a laboratory stand organized for this purpose. The experiment allowed a comparison of flow curves obtained with the use of the constructed device and a standard magnetic-inductive flow sensor SM6000 [1]. The last part of the work contains the analysis of the measurements results, as well as the evaluation of the limiting error of the uroflowmetry device [2, 3].

Keywords: strain gage transducer, uroflowmeter, urine flow, flowmeter.

Introduction

Benign prostatic hyperplasia is one of more frequent diseases of men's urinary system. It is diagnosed when the gland volume is over 30 cm^3 and the maximum urinary flow is less than 15 ml/s. It is estimated that the benign prostatic hyperplasia affects about 50% of men aged around 50 [4]. The high frequency of the disease brings the necessity of working on devices supporting medical diagnostics in this field. The worked out diagnostic unit consists of functional modules, a set of supporting devices and a computer measurement system.

Measurement system

The measurement system was implemented on the base of the platform, in which the first functional module (Fig. 1) is a fluid dispenser. It includes a container and an electromagnetic valve which initiates the flow of the fluid. Because of the comparative character of the research, water was used as the fluid in the measurement system.

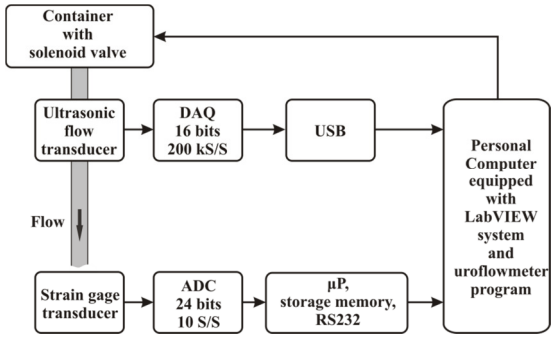

Fig. 1. Measurement system diagram

Another module is the system of the magnetic-inductive flow sensor integrated with a PC by a 16 bit data acquisition card. This part of the system is responsible for measurement data acquisition from the flow meter and its further processing with the use of the LabVIEW program. The SM6000 magnetic-inductive flow sensor takes the role of reference device whose results of the measurements can be compared with the results achieved from the developed instrument. The last element of the laboratory stand is the uroflowmeter itself. It works in the mode which enables independent data storage. The data from the device is read and analyzed in the software made with the use of the C++ language.

Research results

As the result of the research, flow characteristics of a uroflowmeter and an magnetic-inductive flow sensor were determined. In order to present achieved differences for both devices, the most unfavorable case, which occurred during the experiments, was chosen (Fig. 2).

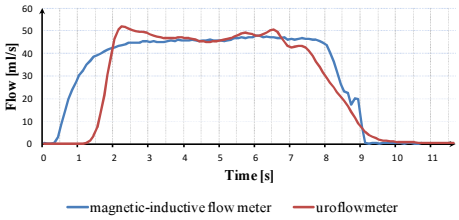

Fig. 2. Uroflowmeter and magnetic-inductive flow meter stored flows

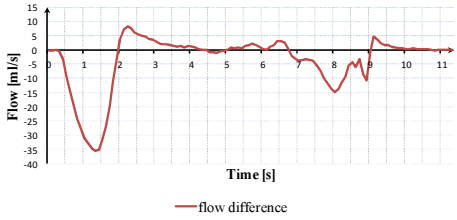

Fig. 3. Achieved flow difference between uroflowmeter and magnetic-inductive flow meter

As it can be observed in Fig. 3, the maximum difference of values appeared in the early phase of flow. This was caused by the fact that the flow meter was placed about 1,5 m away from the weight transducer of the uroflowmeter. In the middle of the section, the maximum difference of the flows equaled about 10 ml/s, and in the final part of the characteristics it was about 18 ml/s.

It can be noticed that the flow measured with the use of the magnetic-inductive device should finish earlier. The main reason of these abnormalities is the lack of synchronization of a sampling time of the analog to digital converter of the uroflowmeter device and the SM6000 sensor. The time difference between achieved samples was nearly 7 ms. It can be accepted as a negligible error while taking into account the duration of micturition, which lasts up to 60 seconds. Yet another factor of the difference can be observed. This is a small amount of the fluid remained in the conducting pipe which is gradually dropped gravitationally with a delay.

Conclusions

The research showed that the constructed uroflowmeter indicates the flow values properly. A small difference between flows, which was observed, can be reduced by proper synchronization of the sampling rate of the analog to digital converter built-in the uroflowmetr device. Despite these minor shortcomings, it was shown that due to the use of the weight transducer, it was possible to work out a construction resistant to temporary flow disappearance which can occur at miction disturbances. Further works will aim at researching the influence of the shape of the forming container (funnel) on the urine flow to the collecting container.

Acknowledgements

The work has been done within the Bialystok University of Technology project S/WE/3/08.

References

[1] Magnetic-inductive flow meter SM6000, Datasheet, http://www.ifm.com/

[2] **Abrams, P.,** Urodynamics, Springer, 1997.

[3] **Makal J., Idźkowski A., Walendziuk W.,** Computer assisted uroflowmetry diagnostic system, Photonics Applications in Astronomy, Communications, Industry, and High-Energy Physics Experiments 2006, Proceedings of SPIE Vol. 6347, Warsaw 2006.

[4] **eMedicine** – Transurethral Microwave Thermotherapy of the Prostate (TUMT) : Article by Jonathan Rubenstein, http://www.emedicine.com/med/topic3070.htm

Weight measurement platform based on a double current supplied circuit and the load cells

Wojciech Walendziuk[1], **Adam Idzkowski**[2]

[1, 2]Bialystok University of Technology, Wiejska 45D str., Bialystok, Poland
E-mail: [1]*w.walendziuk@pb.edu.pl*, [2]*a.idzkowski@pb.edu.pl*

Abstract. The article presents a weight measurement platform in which the original supplying circuit of strain gage load cells is applied. The signal conditioner enables, in a simple way, transformation of the measurement device into a stabilographic platform. The paper discusses construction of the supply system, the way of strain gage transducer connection, the measuring procedure and the analysis of the measurement uncertainty.

Keywords: strain gage transducer, stabilography, weight measurements.

Introduction

The purpose of this paper is to present an alternative switching circuit supply of the resistance strain gages which were applied in the patient's weight measurement device. Moreover, the use of the presented weight transducers supply system enables conducting measurements that, after the appropriate processing, can represent a sought mass. Thanks to this solution of the measurement circuit it will be possible to implement this system into a stabilographic platform [1÷4].

Measurement system

The measurement system was implemented in the platform, in whose corners the one-sidedly fixed beam was placed (Fig. 1). For each of the cantilever beam, on which the strain gage was placed, the strain was examined. Thanks to that it was possible to calculate the applied load.

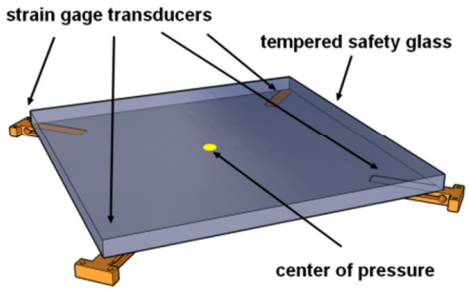

Fig. 1. General view of the measurement platform

Strain gage transducers T_1, T_2, T_3, T_4, were supplied by the circuit in which electronic keys K_1, K_2, K_3, K_4 were used. As shown in Fig. 2, the opposite arms of the bridge power supply include two DC current sources J_1, J_2 and auxiliary resistors R_1, R_2. The complete bridge system consists of the two current sources, two resistors, four strain gage transducers and four electronic keys.

In each measurement cycle, with the use of suitable enabling or disabling state of the electronic keys, it is possible to measure voltage values for determining the expected patient's weight. For example, to determine the mass applied to the platform, firstly a proper combination of enabling electronic switches should be used. First step is to calibrate (tare) the platform with

the use of serial sequence from switch K_1 to K_4. Then it is possible to determine the arithmetic mean value of the applied force, which can be easily converted to mass, while working through the measurements of the voltage drops at each strain gage sensors.

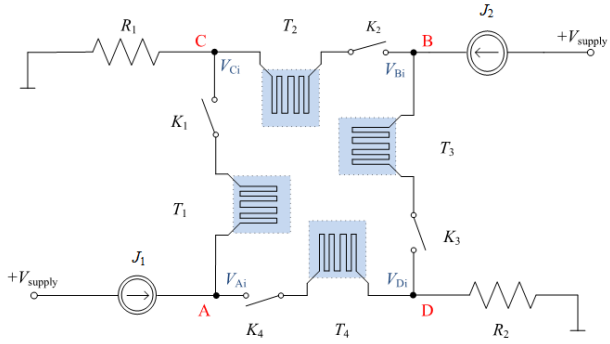

Fig. 2. The way of the strain gage transducers supply and voltage drops measurement

Research and achieved results

During the research, a series of measurement experiments was completed. The aim was to examine the repeatability of determining the mass value at different values of force F applied at the central point of the platform. In order to do it, weights of 2, 5 and 10 kg (which correspond with $F = 20$, 50 and 100 N force values) were placed in the geometrical centre of the plate. There were 5 measurements in each series of experiments followed by evaluating the uncertainty of measurements. The evaluation was conducted through calculating the value of standard deviation, which was done according to the following formula:

$$\sigma(\bar{m}) = \sqrt{\frac{\sum_{k=1}^{N}(m_k - \bar{m})^2}{N(N-1)}} \tag{1}$$

where m is the mass and N is the number of samples.

Conclusions

The results of the experiments were satisfactory. The maximal value of standard deviations for $m = 2$, 5 and 10 kg do not exceed 5% of the applied load. The following stage of the research will be examining the uncertainty of measurements for greater loads (such as 100÷150 kg). It is also planned to work out a stabilographic platform integrated with a PC with the use of the LabVIEW system.

Acknowledgements

The work has been done within the Bialystok University of Technology project S/WE/3/08.

References

[1] **Winter D.A.** Biomechanics and Motor Control of Human Movement**,** Fourth Edition, Wiley & Sons, 2009.

[2] **Walendziuk W., Idźkowski A.** Evaluation of the Static Posturograph Platform Accuracy. Journal of Vibroengineering, Vol. 11, Issue 3, 2009, p. 511–516.

[3] **Augustynek M., Penhaker M., Sazel P., Korpas D.** Stimulation Parameter Testing and Verification during Pacing. IFMBE Proceedings Vol. 29, 2010, p. 533–536.

[4] **Bobbert M., Schamhardt H.** Accuracy of Determining the Point of Force Application with Piezoelectric Force Plates, J. Biomechanics, Vol. 23, No. 7, 1990, p. 705–710.

The associations between variables and support moment in typical children

Jolanta Pauk[1] **, Joanna Szymul**[2]

[1, 2]Bialystok University of Technology, Poland
E-mail: [1]*j.pauk@pb.edu.pl,* [2]*joanna.szymul@tlen.pl*

Abstract. The support moment is defined as the sum of all joint moments in the lower extremity. Positive values are regarded as extensor moments which prevent collapse and negative values as flexor moments which facilitate collapse. The purpose of the study was to determine associations between chosen variables and support moment in typical children population.

Keywords: typical children, regression analysis, support moment, gait analysis.

Introduction

The support moment is defined as the sum of all joint moments in the lower extremity. Positive values are regarded as extensor moments which prevent collapse and negative values as flexor moments which facilitate collapse [1]. The lower limb joint moment is determined by using Newton-Euler equations [2]. The purpose of the study was to determine associations between chosen variables and support moment in typical children population.

The study examined 92 control children. Inclusion criteria were: age range 5–16 years without any disorders that would affect their gait. The study received ethical approval in accordance with the local health committee. All parents provided informed consent prior to the start of measurement. Each child's height was measured to the nearest 0.1 cm using a stadiometer, and the mass of each child was measured to the nearest 0.05 kg using calibrated electronic scales. The natural gait pattern was assessed in the sagittal plane of movement. Reflective markers were placed on the body according to the Oxford model [3]. The subjects were analyzed while walking barefoot. The kinematic and kinetic data were obtained with an optoelectronic system consists of 6 cameras and two platforms. The joint moment at the hip, knee and ankle was computed using an inverse dynamic approach, and then the support moment and the contributions to the support moment was calculated using Eqs. 1 [4]:

$$\overrightarrow{M_s} = \overrightarrow{M}_H + \overrightarrow{M_K} + \overrightarrow{M_A}, \tag{1}$$

where: $\overrightarrow{M_s}$ is support moment, Nm/kg; $\overrightarrow{M}_H$ is hip moment during the stance phase, Nm/kg; $\overrightarrow{M}_K$ is knee moment during the stance phase, Nm/kg; $\overrightarrow{M}_A$ is ankle moment during the stance phase, Nm/kg.

The joint moment was normalized to the body mass. For determining the joint's participation in the support moment the area under the curve of suport moment for the hip joint, knee joint, and ankle joint was calculated as below [4]:

$$\int_{t_1}^{t_2} \overrightarrow{M_s}(t)dt = \int_{t_1}^{t_2} \overrightarrow{M}_H(t)dt + \int_{t_1}^{t_2} \overrightarrow{M}_K(t)dt + \int_{t_1}^{t_2} \overrightarrow{M}_A(t)dt, \tag{2}$$

where: t_1, t_2 is the time of signal duration.

The support moment curve has the characteristic double bump. It is very similar to vertical ground reaction force [4]. A regression approach was used to estimate associations between support moment and chosen variables during walking [5]. Possible independent variables included: body mass, body height, walking speed, single support phase, double support phase, vertical ground reaction force, gender, stride length, and step length. The number of predictors included in the multiple regression models was limited to three predictors due to high correlation between independent variables [5]. Significant effects and the degree of correlation between independent and dependent variables were examined using the Spearman's rank correlation. Finally, dependent variables were as follow: step length normalized to body height (denoted as x_1), maximal vertical ground reaction force normalized to body weight (denoted as x_2), and single support phase (denoted as x_3). The dependent variable was support moment. The following regression equation was as follow:

$$\hat{y} = 51.3 - 4.31x_1 + 4.62x_2 - 4.51x_3 + 8.2x_2x_3 + 5.6x_2^2 - 3.6x_3^2. \quad (3)$$

where: $\hat{y}$ is the dependent variable (model output), $x_1 \ldots x_3$ are the independent variables (model inputs), $a_1 \ldots a_3$ are model coefficients.

Coefficients were assumed to have no significant impact on the output if their p-values were greater than 0.05. Accuracy was examined using root mean square error (RMSE) between measured y and predicted data $\hat{y}$. The model was fitted the measured in 88%. The results indicate that maximal vertical ground reaction force has the highest impact on support moment in typical subjects. Lower impact has step length and single support phase.

Conclusions

This study showed that support moment in typical subjects depends significantly on maximal vertical ground reaction force, step length, and single support phase. The influence of the presented factors on support moment was estimated by a multiple regression model. The proposed method can be used to determine the difference in support moment in children with lower limbs deformities.

Acknowledgements

The paper is supported by the European Union within the confines of the European Social Fund, and Polish Ministry for Science and Higher Education.

References

[1] **Winter D.** Overall principle of lower limb support during stance phase of gait. J Biomech., Vol. 13, 1980, p. 923–927.

[2] **Winter D.** The biomechanics and motor control of human gait normal. Elderly and Pathological. Waterloo University of Waterloo Press, 1991.

[3] **Stebbins J.** *et al*. 2006. Repeatability of a model for measuring multi-segment foot kinematics in children. Gait & Posture, Vol. 23, Issue 4, 2006, p. 401–410.

[4] **Pauk J.** , **Griškevičius J.** Ground reaction force and support moment in typical and flat-feet children. Mechanika, Vol. 17, Issue 1, 2011, p. 93–96.

[5] **Sen A.**, **Srivastava, M**. Regression analysis. Theory, methods and applications. Springer-Verlag, New York, 1990.

Pulse Wave Propagation in Arterial Beds of Upper Extremities: Comparison of 1d and 2d Models

Natalya Kizilova

Kharkov National University, Ukraine
E-mail: *n.kizilova@gmail.com*

Abstract. Pulse wave propagation in the arterial systems of upper extremities is studied on nonlinear 1D and linearized 2D mathematical models. Three types of palm arches are considered. The pressure-flow curves in each artery are computed on 1D and 2D models and compared. It is shown the non-linear terms in 1D model lead to asymmetry of the pressure-flow curves, while the wave dispersion proper to the viscoelastic 2D model are negligible. Novel model-based approaches for the clinical pulse wave diagnostics are proposed.

Keywords: hemodynamics, arterial system, blood flow, pulse wave, medical diagnostics.

Introduction

Pulse wave analysis is a sensitive tool for early medical diagnostics [1, 2]. Anatomy of the arterial bed of upper extremity has some topological variations [3] that can influence pulse wave parameters [4]. The brachial artery (B) divides into radial (R) and ulnary (U) arteries that can be then connected by one A_1 or two $A_{1,2}$ arcs (Fig. 1a-c). Total impedances of the digital arteries are introduced as complex values Z_{1-4}. Since detailed geometry of the palmar arteries is individual and is used for personal identification, the studied problem is important. In the paper pulse wave propagation and reflection in the arterial beds without arcs (Fig. 1a), with one arc (Fig. 1b) and with two arcs (Fig. 1c) is studied on nonlinear 1D and linearized 2D models.

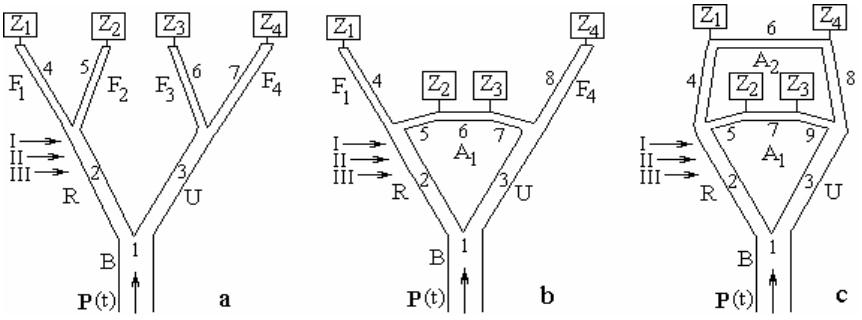

Fig. 1. Arterial systems of upper extremity without arcs (a), with one (b) and two (c) palmar arcs

Problem formulation and solution

Womersley model of 2D axisymmetric pulsatile flow is considered [1]. Each vessel is treated as a viscoelastic tube of length L_j, radius R_j and wall thickness h_j, where j is the serial number of the vessel in the complex branching system (Fig. 1a-c). Pressure $P_j(t,x_j)$ and volumetric rate $Q_j(t,x_j)$ in the j-th tube are introduced as [1]:

$$P_j(t,x_j)=P_j^0 e^{i\omega t}\left(e^{-i\omega x_j/c_j}+\Gamma_i e^{i\omega(x_j-2L_j)/c_j}\right), \qquad (1)$$

where $Z_j^0 = \frac{\rho c_j}{\pi R_j^2}$, $c_j = \left(\frac{E_j h_j (1-F_j)}{2\rho R_j (1-\sigma_j^2)} e^{i\theta_j} \right)^{1/2}$, $F_j = \frac{2J_1(\beta_j)}{\beta_j J_0(\beta_j)}$, $P_j^0 = P_j\big|_{x_j=0}$, $\alpha_j = R_j \sqrt{\frac{\omega\rho}{\mu}}$, $\beta_j = \alpha_j i^{3/2}$, $i = \sqrt{-1}$, Γ_j are unknown reflection coefficients at the tubes' ends, $x_j \in [0, L_j]$ is the longitudinal coordinate along the tube number j, θ_j is dimensionless viscosity of the wall, ρ, μ are density and viscosity of the fluid, ω is angular frequency. Pressure and flow continuity conditions at each bifurcation are

$$Q_i(t, L_i) = Q_j(t,0) + Q_k(t,0), \qquad P_i(t, L_i) = P_j(t,0) = P_k(t,0) \tag{2}$$

where i, j, k are numbers of vessels in a bifurcation. At the inlet of the system $x_1 = 0$ the pressure wave $P_1(t,0) = P_1^0 e^{i\omega t}$ is given. From (1)–(2) one can obtain a nonlinear system of algebraic equations for Γ_j, P_j^0. For different geometrical models (Fig. 1a-c) the pressure distributions along $x_3 \in [0, L_3]$ have been calculated after numerical solution of the nonlinear system by modified Newton's method [4].

1D model is presented by Euler equations with additional drug term produced by viscosity and solved by the method of characteristics [5].

Conclusions

Calculations for (1)–(3) have been carries out at wide variations of Z_j, L_j, R_j and wall material properties E_j, θ_j in accordance with experimental data [1, 4, 5]. The position of the pulse wave diagnostic area at the patient's wrist has been chosen as $x_I = L_3 - l$, $x_{II} = L_3 - 2l$, $x_{III} = L_3 - 3l$, where $l = 1$ cm, the fluid and wall material properties as well as $\mathrm{Re}(Z_j)$, $\mathrm{Im}(Z_j)$ have been chosen within the physiological range [1].

For wide variations of P_1, ω no essential differences between the models a, b, c have been found, which is in agreement with [5]. Additional arches produces backward running wave and the superposition of the forward and backward waves increases the amplitudes of the pulse curves. The results substantiate the possibility of the pulse estimation without preliminary information on the individual structure of the arterial bed of upper extremity of a patient. Atherosclerosis, occlusions, blood insufficiency can be detected by comparative analysis of the pressure and flow waves measured on both arms.

References

[1] **Milnor W.R.** Hemodynamics. Williams &Wilkins, Baltimore, 1989.

[2] **Hammer L.** Chinese pulse diagnosis: A contemporary approach. Eastland Press, 2000.

[3] **Luzsa D.** X-Ray Anatomy of the Vascular System. Acad. Kiado, Budapest, 1973.

[4] **Kizilova N.** Pulse wave reflections in branching arterial networks and pulse diagnosis methods. J. Chinese Inst. Engineers, Vol. 26, 2003, p. 869–880.

[5] **Alastruey J., Parker K.H., Peiro J., Sherwin S.J.** Can the modified Allen's test always detect sufficient collateral flow in the hand? A computational study. Computer Meth. Biomech. Biomed. Eng. Vol. 9, 2006, p. 353–361.

Spectral analysis and mathematical model of human postural sway in sagittal and corollary planes

Natalya Kizilova[1], Julius Griškevičius[2], Michail Karpinsky[3], Elena Karpinskaya[4]

[1]Kharkov National University, Ukraine
[2]Vilnius Gediminas Technical University, Lithuania
[3, 4]M.I.Sytenko Institute of Spine and Joints Pathology, Ukraine
E-mail: [1]*n.kizilova@gmail.com,* [2]*julius.griskevicius@vgtu.lt*

Abstract. Trajectories of the center of pressure (COP) of human body during different stances measured on healthy individuals and patients with spine and joint diseases have been measured. Fourier and continuous wavelet transforms have been used for statistical analysis of the trajectories and 3d representation of the spectral power density (SPD) in both frequency and time domains. The corresponding multilink models have been analyzed and the influence of fixation or pathology of separate joints have been studied. Novel indexes for clinical diagnostics of joint pathologies have been proposed.

Keywords: posturography, postural sway, spectral analysis, biomechanics, clinical diagnostics.

Introduction

Postural sway is important determinant of human locomotor, balance and nervous systems [1]. Sway analysis is used for differential diagnostics of muscular, skeletal, vestibular, nervous, auditory and visual pathology, age-related changes, and emotional state of the individual and alcohol uptake [2, 3]. Body sway in the sagittal plane is quite well studied as an inverted multilink pendulum [1–3], while sway in the corollary plate is not well studied.

Experimental measurements

Posturographic measurements have been done in M.I. Sytenko Institute of Spine and Joints Pathology (Kharkov, Ukraine) on young healthy volunteers and a group of patients with different spine and joint diseases using the force platform (Statograph-M05/28). The series of tests include 2-leg and 1-leg stances with open and closed eyes, normal and fixed joints. Experimental setup is described in [2, 3].

Data analysis

The trajectory $Y_{COP}(X_{COP})$ of the centre of pressure have been computed from the measured time series $(X_{COP}(t),Y_{COP}(t))$. The data have been amplified and the low ($f<0.01$ Hz) and high ($f>10$ Hz) frequency components have been subtracted using the 6-th order Butterworth filter. The 30 s test was split into 4 consequent periods to study the sway amplitudes a_1, a_2, a_3, a_4 and stance regulation at the beginning and at the end of the test. It was shown the body sway amplitude in both sagittal and coronal plate is twice bigger when the eyes are closed and visual control is absent. It was also shown in young healthy individual sway amplitude in bigger in the sagittal plane while in elderly patients with locomotor problems the sway amplitude in the corollary plane may exceed the amplitude in the sagittal plane. Fourier and continuous wavelet transforms have been used for statistical analysis of the trajectories and 3d representation of the spectral power density in both frequency and time domains (Fig. 1). The area A_r of rectangle surrounding the trajectory, trajectory spot area A_s, axes and asymmetry parameters have been computed as well as dynamic velocities dX_C/dt, dY_C/dt and accelerations d^2X_C/dt^2, d^2Y_C/dt^2. According to the second law of dynamics acceleration is proportional to the resulting force produced by the muscles that participate in the balance control.

Mathematical model

Human body is modelled as an inverted 4-link pendulum (Fig. 2). The lengths L_{1-4}, masses M_{1-4}, moments of inertia I_{1-4}, and positions of the centre of mass C_{1-4} determined by distances d_{1-4} in the local coordinate system connected with each segment has known from measurements and tables. Position of the pendulum is determined by angles θ_{1-4} (Fig. 2). Oscillations of the pendulum are described by Lagrange equations. Kinetic and potential energy have been computed for each segment and substituted in Lagrange equations. Supposing the small variations of the angles θ_{1-4} and setting $\sin(\theta_j) \sim \theta_j$, $\cos(\theta_j) \sim 1$ and neglecting terms $\sim (\theta_j)^2$ one can obtain the system of ODE governing oscillations of the links

$$M \cdot \frac{d^2}{dt^2}\vec{\theta} + K(\frac{d}{dt}\vec{\theta}, \vec{\theta}) + N \cdot \vec{\theta} = \vec{u}(\frac{d}{dt}\vec{\theta}, \vec{\theta}) \qquad (1)$$

where $\vec{\theta}^T = (\theta_1, \theta_2, \theta_3, \theta_4)$, sing T denotes transposition, M is the mass-inertia matrix, K is centrifugal matrix, N is gravity matrix, $\vec{u}$ is the control function which is usually supposed to be proportional to deviations of angles and velocities.

Components of the matrices M, K, N are long complex expressions which are not presented here. Nonlinear system (1) has been solved and amplitudes and frequencies of body oscillations have analyzed.

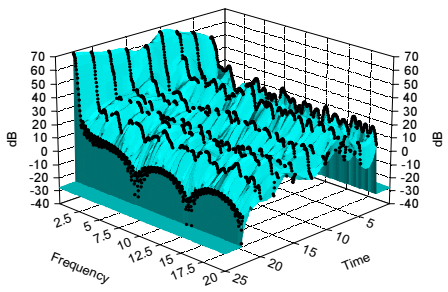

Fig. 1. Dependence of SPD on frequency and time

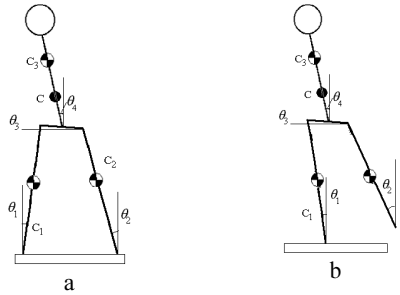

Fig. 2. Multilink models of the human body for the 2-leg (a) and 1-leg (b) stances

Results and discussions

Good agreement of the computed frequencies and measured by spectral analysis of the experimental data have been obtained. It was shown in the young healthy patients a good approximation of the computed results to the measured data is given by the control function determined as $u_j(t) = a\theta_j(t) + bd\theta_j(t)/dt$ while in the elderly patients $u_j(t) = a\theta_j(t-\tau) + bd\theta_j(t-\tau)/dt$ and time delay τ correlates with both age and pathology level. It is shown the parameters A_s/A_r, $a_1{:}a_2{:}a_3{:}a_4$ and $SPD_1{:}SPD_2{:}SPD_3{:}SPD_4$ for 4 consequent test periods gives important information for early diagnostics of postural disorders.

References

[1] Zatsiorsky V.M., Aruin A.C., Selujanov V.N., *Biomechanics of human locomotor system,* Moscow, 1981.

[2] Karpinsky M.Yu., Kizilova N.N., *Computerized posturography for data analysis and mathematical modelling of postural sway during different 2-legged and 1-legged human stance*, J. Vibroeng., 2007, 9, 118–124.

[3] Kizilova N., Karpinsky M., Griskevicius J., Daunoraviciene K., *Posturographic study of the human body vibrations for clinical diagnostics of the spine and joint pathology*, Mechanika, 2009, 6, 37–41.

Data mining in analyzing pressure on plantar surface in children gait

M. Derlatka[1], **M. Ihnatouski**[2]

[1]Bialystok University of Technology, Bialystok, Poland
[2]Center of Resource Saving. Belarusian Academy of Science, Grodno, Belarus
E-mail: [1]*m.derlatka@pb.edu.pl*, [2]*mii_by@mail.ru*

Keywords: posturography, postural sway, spectral analysis, biomechanics, clinical diagnostics.

Introduction

Data mining is the set of methods which enables to manage a huge and multidimensional set of measured data. Data mining provides for fast and efficient analyzing of the data and finding new, sometimes unexpected, connections between various parameters [3]. One of the important problems is an automatic instrumented human gait analysis. Gait is very complex human activity which could be described by enormous number of parameters. The measurement of some of those parameters is necessary to perform the quantitative human gait assessment. Nowadays, the methods of automatic human gait analysis are very popular, because they break the limitations of manual evaluation of the data concerning gait [1], [2]. The good example of such problem could be handling with children with pes planovalgus (PP). Pes planovalgus is one of the most frequently appearing foot diseases. In this case the foot has a small, longitudal arch while loading. It is a result of the muscular-ligament system failure. Moreover in pes planovalgus the heel bone is in the pronation position while results from the foot being more flattened. The results of pes planovalgus are foot deformation and pain. It shows that the children should be correctly diagnosed and they should start therapy as soon as possible. The data mining methods could be very helpful in constructing the support decision making system.

One of the most promising techniques of data mining is decision tree. Decision trees enable to extract the knowledge hidden in the data and presenting it in a very vivid way. They provide very simple conditions in the tree nodes and lead to conclusion (class) on the lowest level of the tree. It is very important that the results are easy for interpretation and could be used by the staff with neither mathematical nor engineering background. Decision trees have already been successfully used in the human gait analysis in clinical applications [2].

This paper describes the application of decision tree to the analysis of biomechanical signals. The main aim of the analysis of those signals is to demonstrate the possibility of the diagnosis, which utilizes recorded signals describing the gait of the investigated subject by means of decision tree.

Materials and Method

The foot pressure measuring system is one of the most common devices for human gait analysis. The devices of this type are often used in foot pathologies. During the investigation the barometric insole of an appropriate size is put into the subject's shoes. The insoles consist of capacitive sensors (max 240 sensors per insole), which allow to record with frequency of 300 Hz the distribution of pressure of the human plantar onto the contact surface while walking. We made measurements based on a group of 20 children (10 children with PP and 10 children as a reference group with typical foot). The subjects walk along a pathway in a comfortable self-determined way. Thus, for the single subject many strides of human gait have been recorded (260 strides: 140 strides for control group and 120 strides for children with PP). The subjects who took part in the investigations were at age 14.3 ± 5.93 (PP group) and 15.0 ± 1.69 (control group), body weight:

44.4 ± 11.46 kg (PP) and 53.25 ± 9.15 kg (control). We grouped insole sensors seven anatomic zones (Z) (Fig. 1). Zone 1 is equivalent to toes, 2 metatarsal heads (from 2nd to 5th), 3 head of 1st metatarsal, 4 cuboid bone, 5 navicular bone, 6 lateral heel and 7 is an internal heel.

We divide the recorded time series into parts. The parts are the phases which are present in normal support phase of gait. They were: loading response (0–10% of gait cycle), Mid Stance (10%–30%), Terminal Stance (30%–50%), PreSwing (50%–60%). We have calculated the following parameters for the every zone end every gait phase: the average value of absolute pressure; the average value of pressure normalized to body weight; the time of i^{th} zone contact and the percent of participation the i^{th} zone in whole foot loading. Moreover recorded strides has been divided into two sets: learning set (185 strides) – which was used for building decision tree and testing set (75) – which was used to check the quality of the system. In this paper we build decision tree based on the CART algorithm and Gini's index. A 10-fold cross validation was used to prevent from over fitting of the decision tree.

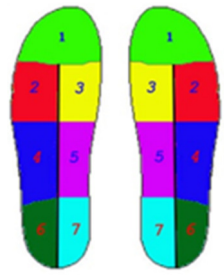

Fig. 1. The sensors insole divided into anatomic zones

Results

The result of using the CART algorithm was a decision tree with 11 nodes (6 conslusion nodes) (Fig. 2). The rate of correct classification is quite good: 95% for reference group and 93% for PP one in case of training set and 95% for reference group and 83% for PP group. It is easily to notice that the most important for decision making are two gait phases: Mid Stance (and Pre Swing. It should be underline that during MidStance phase of gait a foot is in full load and in fact the pathological position of foot should be the most noticeableat that time. Very important in distinguishing those two group are zones connected to internal side of the foot (zone 5 and zone 7). It is connected with pronation of foot in case of the pes planovalgus subtects.

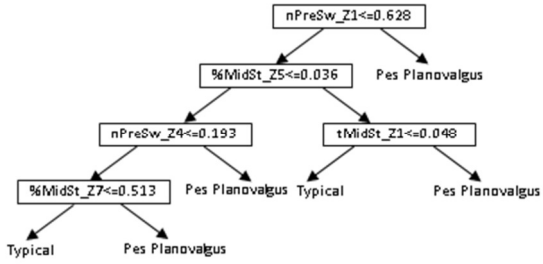

Fig. 2. The obtained decision tree

Conclusions

The results demonstrate that decision trees are a powerful technique which could be successful applied in analyzing pressures on plantar surface in children gait. The advantage of employing decision trees is the easiness of results interpretation. Constructing a decision tree could help in finding the associations between measured data and undertaken decision. Decision trees could improve the understanding of human gait phenomenon.

References

[1] **Chau T**. Review of analytical techniques for gait data. Part 1: fuzzy, statistical and fractal methods. Gait and Posture 13, 2001, p. 49–66.

[2] **Derlatka M., Ihnatouski M**. Decision tree approach to rules extraction for human gait analysis. ICAISC'2010 LNCS Vol. 6114: LNAI, 2010, p. 597–604.

[3] **Hand D., Mannila H., Smith P**. Principles of data mining. Polish edition. WNT, Warsaw 2005.

Authors Index